

AD-A203 805

FINAL REPORT  
Contract No. N00014-86-C0313

SULFIDE AND PHOSPHIDE ANALOGS OF  
OXYNITRIDE CERAMICS

to

NAVAL WEAPONS CENTER  
OFFICE OF NAVAL RESEARCH  
800 N. Quincy Street  
Arlington, Virginia 22217

January 17, 1989

by

Dr. Peter J. Melling

BATTELLE  
MEMORIAL INSTITUTE  
505 King Avenue  
Columbus, Ohio 43201-2693

DTIC  
ELECTE  
S JAN 25 1989 D  
H

DISTRIBUTION STATEMENT A

Approved for public release;  
Distribution Unlimited

REPORT DOCUMENTATION PAGE

1a. REPORT SECURITY CLASSIFICATION <b>Unclassified</b>		1b. RESTRICTIVE MARKINGS	
2a. SECURITY CLASSIFICATION AUTHORITY		3. DISTRIBUTION / AVAILABILITY OF REPORT <b>Unlimited</b>	
2b. DECLASSIFICATION / DOWNGRADING SCHEDULE		5. MONITORING ORGANIZATION REPORT NUMBER(S)	
PERFORMING ORGANIZATION REPORT NUMBER(S) <b>Final Report</b>		7a. NAME OF MONITORING ORGANIZATION <b>Naval Weapons Center</b>	
4a. NAME OF PERFORMING ORGANIZATION <b>Battelle Memorial Institute</b>	6b. OFFICE SYMBOL (If applicable)	7b. ADDRESS (City, State, and ZIP Code) <b>Code</b>	
4c. ADDRESS (City, State, and ZIP Code) <b>505 King Avenue Columbus, Ohio 43201-2693</b>		9. PROCUREMENT INSTRUMENT IDENTIFICATION NUMBER <b>N00014-86-C0313</b>	
5a. NAME OF FUNDING / SPONSORING ORGANIZATION <b>Office of Naval Research</b>	8b. OFFICE SYMBOL (If applicable)	10. SOURCE OF FUNDING NUMBERS	
5c. ADDRESS (City, State, and ZIP Code) <b>800 N. Quincy Street Arlington, Virginia 22217</b>		PROGRAM ELEMENT NO.	PROJECT NO.
		TASK NO.	WORK UNIT ACCESSION NO.
11. TITLE (Include Security Classification) <b>Sulfide and Phosphide Analogs of Oxynitride Ceramics</b>			
12. PERSONAL AUTHOR(S) <b>Peter J. Melling</b>			
13a. TYPE OF REPORT <b>Final</b>	13b. TIME COVERED FROM <b>86/3/19</b> TO <b>88/11/18</b>	14. DATE OF REPORT (Year, Month, Day) <b>89/1/17</b>	15. PAGE COUNT
16. SUPPLEMENTARY NOTATION			
17. COSATI CODES		18. SUBJECT TERMS (Continue on reverse if necessary and identify by block number)	
FIELD	GROUP	SUB-GROUP	
		IR Domes	
19. ABSTRACT (Continue on reverse if necessary and identify by block number)			
-OVER-			
20. DISTRIBUTION / AVAILABILITY OF ABSTRACT <input checked="" type="checkbox"/> UNCLASSIFIED/UNLIMITED <input checked="" type="checkbox"/> SAME AS RPT. <input type="checkbox"/> DTIC USERS		21. ABSTRACT SECURITY CLASSIFICATION <b>Unclassified</b>	
22a. NAME OF RESPONSIBLE INDIVIDUAL <b>Dr. R. W. Schwartz</b>		22b. TELEPHONE (Include Area Code) <b>(619) 939-1655</b>	22c. OFFICE SYMBOL <b>NWC</b>

ABSTRACT

↓  
 A survey of compositions in the GeGaPS system, initially based on the <sup>β</sup>-Sialon system (Si<sub>4</sub>Al<sub>2</sub>O<sub>2</sub>N<sub>6</sub>) was carried out. Most of the samples were prepared by sealed tube melting (using a fused quartz tube) of mixtures of the elements in a rocking furnace. When it was found that these materials are sensitive to oxygen contamination a pressure melting system was constructed in which melts were prepared in vitreous carbon crucibles under an inert gas overpressure. → *Fig 2*

In the sealed tube work, the products were found to be sensitive to the form in which the starting materials were used, e.g., the use of powdered or lump germanium gave different results, and different oxygen contents were found in the resulting product. Samples were manually examined for mechanical integrity and electrical conductivity. Those which passed were evaluated by DTA and then for thermal expansion. Infrared spectra, were measured and mechanical testing conducted, on selected samples. Solid-state <sup>31</sup>P nuclear magnetic resonance (NMR), was used to estimate the amount of phosphate present in the glasses, and to confirm that the phosphorus was present principally in the desired reduced state rather than in the oxidized or positive state. Detailed examination of the crystallization behavior of GeGa<sub>0.24</sub>P<sub>0.2</sub>S<sub>2</sub> glass was carried out using an electron microprobe. A highly complex microstructure was observed which contained gallium sulfides, germanium sulfides, and zoned mixed crystals of germanium-gallium-sulfide.

In addition, two other materials were briefly examined: the addition of ZnS to the GeGaSP system and ZrS<sub>3</sub> to the GeS system, to give glass ceramics was demonstrated but the materials had thermal expansions which were higher than desired. The overall conclusion is that Sialon-like structures are not readily formed in the GeGaSP system, and that the measured thermal expansions are too great to be of useful for dome materials in severe thermal environments. In particular, no material superior to ZnS was found.

Attention was therefore turned to a study of the potential toughening of ZnS itself by the addition of the softer material ZrS<sub>3</sub>. A fracture toughness of over twice the value for ZnS processed under the same conditions was obtained, without loss of bend strength. Microstructural studies indicate that the mechanism is crack bridging and crack deflection by ZrS<sub>3</sub> stringers and particles. This system strongly merits further study. Also, the thermal expansion of NaLaS<sub>2</sub>, another potential LWIR material was measured and found to be 15x10<sup>-6</sup> °C<sup>-1</sup>.

*Key words: SIALON, OXYNITRIDE CERAMICS, Phosphates, Nuclear magnetic Resonance, INFRARED SPECTRA, Germanium, Gallium, Zirconium Sulfide.*

DTIC COPY INSPECTED

(JIS) ←

Distribution/Availability Codes	
Dist	Avail and/or Special
A-1	

## TABLE OF CONTENTS

	<u>Page</u>
ABSTRACT.....	vii
INTRODUCTION.....	1
EXPERIMENTAL.....	2
Materials Preparation.....	2
Rocking Furnace.....	2
Pressure Furnace.....	4
Hot Pressing.....	4
Materials Evaluation.....	4
Thermal Analysis.....	7
Microstructural Analysis.....	7
Mechanical Testing.....	8
Thermal Expansion Measurements.....	9
Spectroscopic Analysis.....	10
RESULTS.....	11
The Ge-Ga-P-S System.....	11
Crystallization Studies.....	24
Nuclear Magnetic Resonance Studies.....	38
The Ge-Ga-Zn-S-P and Ge-Zr-S Systems.....	41
NaLaS <sub>2</sub> Thermal Expansion.....	51
The ZnS-ZrS <sub>3</sub> System.....	52
Young's Modulus and Bend Strengths.....	52
Fracture Toughness.....	57

TABLE OF CONTENTS (Continued)

	<u>Page</u>
Microstructure.....	59
Toughening Mechanism.....	61
CONCLUSIONS.....	64
REFERENCES.....	65

## LIST OF TABLES

	<u>Page</u>
TABLE 1. GeGaPS Compositions Prepared.....	12
TABLE 2. Annealing Treatments for GeGaPS Glasses.....	34
TABLE 3. Analysis of Large Crystals Formed at 600° C (8 hrs.).....	38
TABLE 4. Summary of <sup>31</sup> P NMR Results.....	41
TABLE 5. GeZnGaPS and GeZrS Compositions Prepared.....	47
TABLE 6. Calculation of NaLaS <sub>2</sub> Lattice Parameters.....	51
TABLE 7. Bend Strengths of ZnS/ZrS <sub>3</sub> Composites.....	56
TABLE 8. Fracture Toughness of ZnS/ZrS <sub>3</sub> Composites.....	57

## LIST OF FIGURES

FIGURE 1. Rocking Furnace.....	3
FIGURE 2. Pressure Furnace System.....	5
FIGURE 3. Carbon Crucible Assembly.....	6
FIGURE 4. DTA of Ge-S <sub>0.5</sub> P Glass.....	13
FIGURE 5. Globular Microstructure of Ge-S <sub>0.5</sub> P Glass.....	14
FIGURE 6. DTA of 0.1 Ga <sub>2</sub> S <sub>3</sub> -GeS <sup>1,2</sup> .....	16
FIGURE 7. DTA of GeS <sub>1.2</sub> Glass.....	17
FIGURE 8. Infrared Transmission Scan of GeGa <sub>0.2</sub> S <sub>1.5</sub> .....	18
FIGURE 9. DTA of GeGa <sub>0.4</sub> S <sub>1.8</sub> Glass.....	19
FIGURE 10. DTA of GeGa <sub>0.2</sub> S <sub>2</sub> Glass Using Powdered Germanium.....	20

LIST OF FIGURES (Continued)

	<u>Page</u>
FIGURE 11. DTA of $\text{GeGa}_{0.2}\text{S}_2$ Glass Using Lump Germanium.....	21
FIGURE 12. DTA of $\text{GeS}_3$ Glass.....	22
FIGURE 13. DTA of $\text{GeS}_4$ Glass.....	23
FIGURE 14. DTA of $\text{GeGa}_{0.25}\text{P}_{0.25}\text{S}_{1.88}$ .....	25
FIGURE 15. $\text{GeGa}_{0.25}\text{S}_{2.5}\text{P}_{0.25}$ Glass.....	26
FIGURE 16. DTA of High Sulfur Glass.....	27
FIGURE 17. DTA of Low Sulfur Glass.....	28
FIGURE 18. DTA of $\text{GeGa}_{0.24}\text{P}_{0.2}$ Glass Melted in the Pressure Furnace.....	29
FIGURE 19. Typical Crystal of GeGaPS Glass.....	30
FIGURE 20. Microstructure of GeGaPS Glass.....	31
FIGURE 21. Zoned Mixed Crystals.....	32
FIGURE 22. "Wheat Sheaf" Morphology.....	33
FIGURE 23. Needle Like Gallium Sulfide Crystals.....	35
FIGURE 24. "Blocky" Crystals.....	36
FIGURE 25. Large Crystals - 8 Hour Anneal.....	37
FIGURE 26. Concentration Profile at The Glass-Crystal Interface.....	39
FIGURE 27. Microstructure of $\text{GeGa}_{24}\text{P}_{0.2}\text{S}$ After 64 Hours at $600^\circ\text{C}$ .....	40
FIGURE 28. NMR Spectrum of $\text{GeGa}_{0.33}\text{PS}_{0.5}$ .....	42
FIGURE 29. NMR Spectrum of $\text{GeGa}_{.25}\text{P}_{.25}\text{S}_{2.5}$ .....	43

LIST OF FIGURES (Continued)

	<u>Page</u>
FIGURE 30. NMR Spectrum of $\text{GeGa}_{0.133}\text{PS}_{0.2}$ .....	44
FIGURE 31. NMR Spectrum of $\text{GePS}_{0.5}$ .....	45
FIGURE 32. NMR Spectrum of $\text{GePS}_{0.2}$ .....	46
FIGURE 33. DTA of $\text{GeZn}_{0.1}\text{Ga}_{0.2}\text{S}_{2.3}$ Glass Ceramic.....	48
FIGURE 34. DTA of $\text{GeZn}_{0.075}\text{Ga}_{0.2}\text{P}_{0.05}\text{S}_{2.2}$ .....	49
FIGURE 35. DTA of $\text{GeZn}_{0.1}\text{Ga}_{0.2}\text{P}_{0.07}\text{S}_{2.2}$ Glass Ceramic.....	50
FIGURE 36. Plot of The Lattice Parameter of $\text{NaLaS}_2$ Powder as a Function of Temperature.....	53
FIGURE 37. Stress-Strain Curve for $\text{ZrS}_3$ .....	54
FIGURE 38. Bend Strengths of $\text{ZnS}/\text{ZrS}_3$ Composites.....	55
FIGURE 39. Fracture Toughness Versus Mole Percent $\text{ZrS}_3$ of $\text{ZnS}/\text{ZrS}_3$ Composites.....	58
FIGURE 40. "Crack Path" of 30 Mole Percent $\text{ZrS}_3$ Fracture Toughness Specimen.....	60
FIGURE 41. Photomicrograph Taken Away From Notch Tip.....	62
FIGURE 42. Higher Magnification of Small Region of Figure 41.....	63

## ABSTRACT

A survey of compositions in the GeGaPS system, initially based on the  $\beta$ -Sialon system ( $\text{Si}_4\text{Al}_2\text{O}_2\text{N}_6$ ) was carried out. Most of the samples were prepared by sealed tube melting (using a fused quartz tube) of mixtures of the elements in a rocking furnace. When it was found that these materials are sensitive to oxygen contamination a pressure melting system was constructed in which melts were prepared in vitreous carbon crucibles under an inert gas overpressure.

In the sealed tube work, the products were found to be sensitive to the form in which the starting materials were used, e.g., the use of powder or lump germanium gave different results, and different oxygen contents were found in the resulting product. Samples were manually examined for mechanical integrity and electrical conductivity. Those which passed were evaluated by DTA and then for thermal expansion. Infrared spectra, were measured and mechanical testing conducted, on selected samples. Solid-state  $^{31}\text{P}$  nuclear magnetic resonance (NMR), was used to estimate the amount of phosphate present in the glasses, and to confirm that the phosphorus was present principally in the desired reduced state rather than in the oxidized or positive state. Detailed examination of the crystallization behavior of  $\text{GeGa}_{0.24}\text{P}_{0.2}\text{S}_2$  glass was carried out using an electron microprobe. A highly complex microstructure was observed which contained gallium sulfides, germanium sulfides, and zoned mixed crystals of germanium-gallium-sulfide.

In addition, two other materials were briefly examined: the addition of ZnS to the GeGaSP system and  $\text{ZrS}_3$  to the GeS system, to give glass ceramics was demonstrated but the materials had thermal expansions which were higher than desired. The overall conclusion is that Sialon-like structures are not readily formed in the GeGaSP system, and that the measured thermal expansions are too great to be of use for some materials in severe thermal environments. In particular, no material superior to ZnS was found.

Attention was therefore turned to a study of the potential toughening of ZnS itself by the addition of the softer material  $\text{ZrS}_3$ . A fracture toughness of over twice the value for ZnS processed under the same conditions was obtained, without loss of bend strength. Microstructural studies indicate that the mechanism is crack bridging and crack deflection by  $\text{ZrS}_3$  stringers and particles. This system strongly merits further study. Also, the thermal expansion of  $\text{NaLaS}_2$ , another potential LWR material was measured and found to be  $15 \times 10^{-6} \text{ }^\circ\text{C}^{-1}$ .

# FINAL REPORT

on

## SULFIDE AND PHOSPHIDE ANALOGS OF OXYNITRIDE CERAMICS

Contract N00014-86-C-0313

January 17, 1989

BATTELLE MEMORIAL  
INSTITUTE  
505 King Avenue  
Columbus, Ohio 43201-2693

### INTRODUCTION

→ There is a requirement for new materials which are transparent in the 8-14 ~~um~~ wavelength range and have superior thermal shock resistance, toughness, mechanical strength, and abrasion resistance compared to existing materials. The purpose of this work was to evaluate the possibility of preparing sulfide-phosphide analogs of oxynitride glasses and glass ceramics in the GeGaPS system. If the silicon nitride structure could be prepared in this system, large improvements in mechanical properties are expected.

The investigation of non-oxide chalcogenide glasses as infra-red optical materials began in 1950 when R. Frerichs<sup>(1,2)</sup> rediscovered  $As_2S_3$  glass. Since then, IR transmitting glasses have been the subject of numerous investigations and are now commercially available and used in IR optical systems. The investigation described in this report examined a number of compositions in the GeGaPS system in an attempt to emulate the highly thermal-shock-resistant SiAlON system. Highly complex crystallization behavior was found in the glasses but no SiAlON type phases were observed.

The philosophy that was followed in this program was to survey a large number of compositions and to study more closely any materials which showed promise. When it became apparent that the phosphorus was very reluctant to occupy nitride-like crystal sites and that the glasses being formed had relatively low glass transition temperatures, some highly successful experiments were conducted to investigate the toughening of ZnS (the current material of choice) with additions of a softer material ( $ZrS_3$ ).

## EXPERIMENTAL

All the materials required for this program were synthesized at Battelle and then subjected to thermal, microstructural, mechanical and optical analysis as appropriate.

### Materials Preparation

Samples were prepared for evaluation by two melting methods: sealed tube melting in a rocking furnace and crucible melting in a pressure furnace, and by hot pressing.

#### Rocking Furnace

A rocking furnace was assembled (Figure 1). This system consists of a 1200°C Marshall tube furnace (89 mm I.D. by 500 mm long) mounted on a bearing and rocked vertically about a center axis on the bottom of the furnace by a small electric motor.

Raw materials were loaded into quartz tubes measuring 6 inches long with a 10 mm I.D. and 3 mm wall thickness and sealed on one end. The wall thickness was 3 mm to reduce the risk of tube failure and the consequent explosion hazard. The loaded tubes were evacuated overnight then sealed while under vacuum using standard glassblowing techniques. The sealed tubes were placed in a stainless steel pipe (for containment in case of explosion) then placed in the furnace.

A typical heating schedule is given below:

20°C	→	900°C	40°C/hr.
900°C	→	950°C	10°C/hr.
950°C	→	1000°C	40°C/hr.
1000°C	→	hold 14 hours.	

Furnace cool to 650°C  
Remove from furnace.

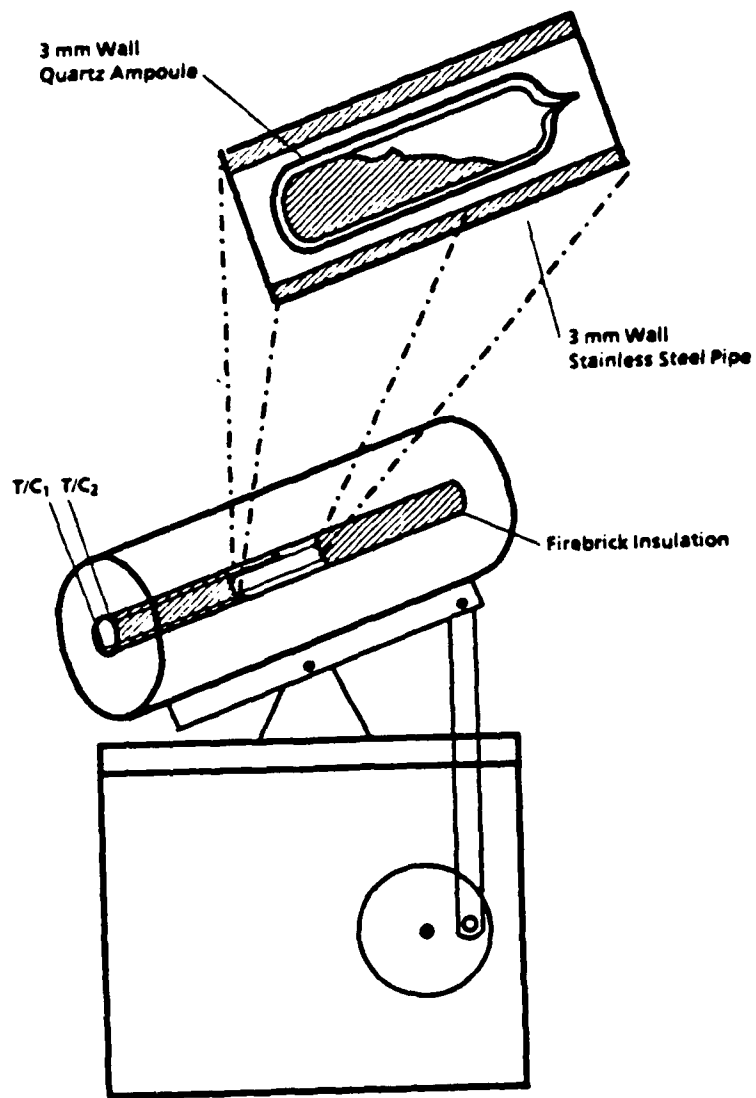


FIGURE 1. ROCKING FURNACE

### Pressure Furnace

In order to eliminate contact between the sample and oxide materials a pressure melting system was developed (Figure 2). The pressure vessel is constructed of SB574-Hastalloy C. The vessel has a 140 mm I.D. and 380 mm inside height. The vessel has thermal insulation on the sidewalls, top and bottom which insulate electrical resistance heating units capable of 1200°C. The maximum working pressure was 4800 psi.

The raw materials were loaded into vitreous carbon crucibles measuring 50 mm x 50 mm diam. The vitreous carbon crucibles were placed into a graphite crucible with double graphite lids as in Figure 3. A double lid arrangement was found to be necessary to limit evaporation losses from the melt. When used it virtually eliminated vapor losses. The crucible assemblies were loaded into the pressure vessel then the vessel was sealed, evacuated, and back-filled with Argon to 1500 psi.

### Hot Pressing

An induction-heated 15 ton vacuum hot press which can accommodate 110 mm OD x 150 mm long dies and is capable of a 2100°C operating temperature was used. Raw materials were blended and loaded into a graphite die lined with Mo foil. Mo foil also protected the sample from the graphite punches. The die and punches were placed in the hot press which was then evacuated and back-filled with argon. The material was heated to 950°C at 10°C/min. At temperature, pressure was applied to yield 103 MPa on the sample. The sample was then held at temperature and pressure for one hour.

### Materials Evaluation

A wide range of characterization techniques were used to evaluate materials produced at Battelle and by other members of the Office of Naval Research (ONR) "Materials for Long Wave Infra-Red Windows and Domes" program. Details of the major analytical methods are given below.

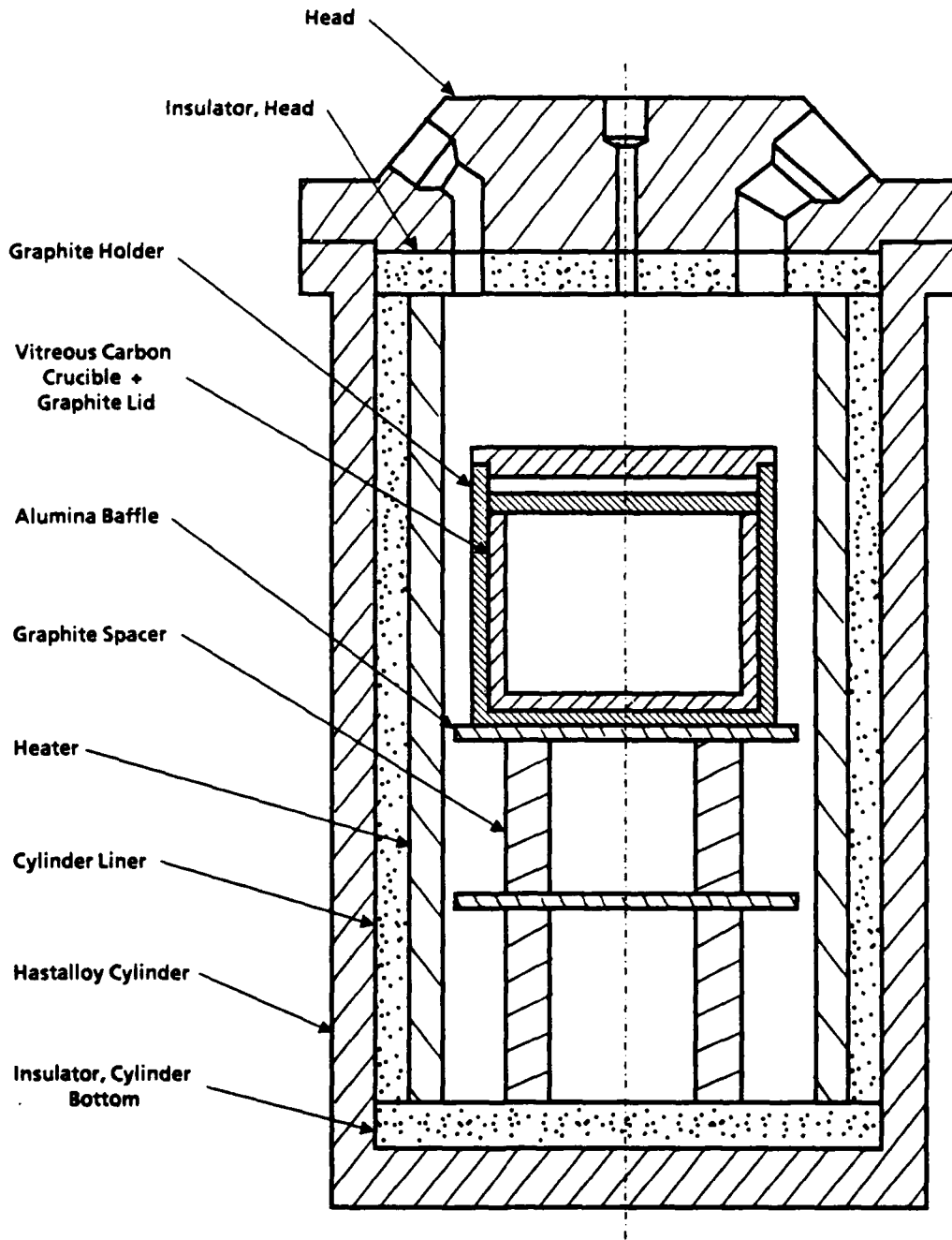


FIGURE 2. PRESSURE FURNACE SYSTEM

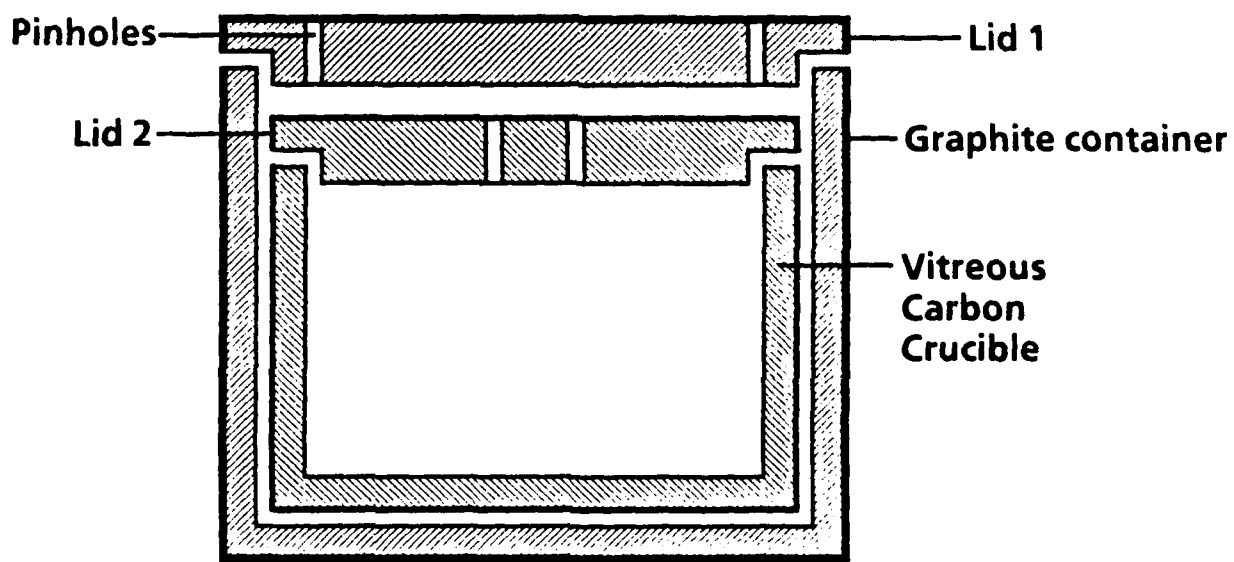


FIGURE 3. CARBON CRUCIBLE ASSEMBLY

### Thermal Analysis

Differential thermal analysis (DTA) was used to determine the crystallization behavior, melting temperatures, and glass transition temperatures of many of the compositions. A Perkin Elmer 1700 DTA unit was used and samples were measured under flowing nitrogen or argon at atmospheric pressure. This was adequate for most samples however some compositions were unstable and tended to foam under ambient pressure giving uninterpretable results at high temperatures. A high pressure DTA cell would be required to deal with this but none was available to us.

### Microstructural Analysis

Electron Probe Microanalysis (EPMA) combines structural and compositional analysis in one operation. The microscope can be used as a scanning electron microscope (SEM), with secondary electron and back-scattered imaging and energy dispersive spectroscopy (EDS), or as a microanalytical tool by using wave dispersive spectroscopy (WDS). EPMA allows the detection of elements with atomic number of 5 (boron) or greater. Its sensitivity in quantitative analysis is ~100 ppm for elements with an atomic number greater than 11 (sodium); this decreases when detecting light elements in a heavy matrix.

A Jeol 733 Superprobe was used to perform the microstructural characterization of the GeGaPS samples. When examined in secondary electron imaging (SEI) mode, it was difficult to distinguish the presence of any phases other than the glass matrix. However, when the samples were examined by back-scattered imaging (BSI), it was possible to see the different phases present. Contrast in BSI is caused by the difference in atomic numbers of the constituents in the sample; elements with a higher atomic number appear as brighter portions of the image. In the case of the GeGaPS glasses, the BSI contrast between germanium and gallium, and similarly between phosphorus and sulphur, is limited because of the closeness of these pairs in atomic number.

However, by optimizing the electron operating voltage and probe current, it was possible to obtain clear images of the different phases.

X-ray fluorescence maps were generated by the use of wavelength dispersive spectroscopy (WDS). Using WDS rather than energy-dispersive spectroscopy (EDS), it was possible to produce high-resolution element distribution maps which gave qualitative information on the spatial distribution of the constituents of the sample.

Compositional analyses performed on some of the samples, were carried out using two WDS spectrometers with a lithium fluoride (LIF) crystal for the germanium and gallium analysis, and a thallium acid phthalate (TAP) crystal for the phosphorus and sulphur analysis. All analyses were calibrated with in-situ standards for each of the elements.

### Mechanical Testing

Bend strengths of hot-pressed samples were determined using a 3-point bend fixture on an Instron testing machine. The distance between the supports was approximately 18 mm, and this length was limited essentially by the available size of the billets. The bend bars had a rectangular cross-section with nominal dimensions 2.5 mm thick by 3.8 mm wide. The orientation of the specimens was such that the tensile and compressive faces of the bend bars lay perpendicular to the hot pressing direction. The testing was done at a cross-head speed of 0.05 mm per minute.

A 4-point bend experiment was performed on one specimen of  $ZrS_3$ , to determine the modulus and strength of the material. The inner and outer supports of the 4-point fixture were 19 mm and 32 mm respectively, and the specimen had a cross-section of approximately 2.3 mm thick by 7.3 mm wide. The specimen was strain-gaged using a 6.35 mm long strain gage that was glued to the tensile surface.

Fracture toughness measurements were made using straight-notched 3-point bend specimens. The width B of the specimens ranged between 3.5 mm and 5.0 mm, while the depth W ranged between 12 mm and 18 mm. A diamond slitting saw was used to introduce a crack, such that the ratio a/W of the crack length

a to the specimen depth  $W$  was approximately 0.4. The width of the notch was approximately 0.38 mm, and no additional efforts were made to introduce a finer crack. Since an objective of the task was to compare the fracture toughness of similar specimens, the finite width of the notch did not pose a major concern.

The orientation of the specimens was chosen such that the crack-front was parallel to the hot-pressing direction, and the crack propagated in a direction perpendicular to the hot-pressing direction. The span  $L$  between the bottom supports was approximately 20 mm. Thus, the ratio of the span to the specimen depth was close to 2, although in regular fracture toughness testing (ASTM E399) a ratio of 4 is preferred. As already mentioned, the length of the samples was limited by the diameter of the billets.

The fracture toughness specimens were loaded at a cross-head displacement rate of 0.05 mm per minute, and the load was recorded as a function of cross-head displacement. Fast fracture was associated with a sudden drop in load. Following the experiments some of the specimens were polished, and micrographs were obtained that illustrated the crack path.

Hardness measurements were made on selected samples by the Knoop indenter method.

### Thermal Expansion Measurements

Thermal expansion was measured by two methods: A Netzch 402E recording dilatometer was used for routine expansion measurements and measurements on glass samples; and variable temperature X-ray diffraction measurements were performed on crystalline materials when highly accurate data was required.

Dilatometer measurements were performed under an inert atmosphere on rod shaped samples or blocks approximately 10 mm long.

A fully automated Rigaku X-ray diffractometer with a high-temperature controlled-atmosphere sample stage was used for this work. The samples were packed into a platinum holder and the sample chamber was purged with helium before the start of the run. A room temperature scan was taken so

that any misalignment errors could be corrected for, then a set of peaks at high angle were selected, which would provide data on all crystallographic axes. The sample was then heated, held at temperature for 30 minutes, the selected peaks scanned, then heated to the next temperature. Full XRD patterns were also taken at more widely spaced intervals to determine whether any sample reaction or decomposition was occurring.

### Spectroscopic Analysis

IR Spectra were measured with a standard Fourier transform instrument either in reflectance mode, for thick or particularly absorbing samples, or in transmission mode on samples usually 2 mm to 3 mm thick.

Phosphorus  $^{31}\text{P}$  nuclear magnetic resonance (NMR) samples were submitted to the Naval Weapons Center where powder samples were measured using magic angle spinning solid state NMR. It was expected that NMR would be useful in determining the oxidation state of phosphorus in glassy samples and also act as an indicator of phosphate contamination.

## RESULTS

As the program developed, three major types of material were investigated. Initially GeGaPS compositions were examined and then, when it became apparent that the desired improvements were not being obtained, additions of ZnS and ZrS<sub>3</sub> to the GeSP system were studied. This then led to the development of ZnS-ZrS<sub>3</sub> composites which we have shown to have toughness superior to that of ZnS without loss in strength.

### The Ge-Ga-P-S System

Initially a series of compositions, chosen by a statistical design around the  $\beta$ -Sialon composition (Si<sub>4</sub>Al<sub>2</sub>O<sub>2</sub>N<sub>6</sub>) were attempted to be melted. The elements (mixed in the appropriate proportions) were placed in a sealed evacuated fused quartz tube and placed in the rocking furnace. With the equipment available we were not able to obtain homogeneous melts and a number of the samples exploded violently. Subsequent remelting of those samples in the pressure furnace did not yield satisfactory melts either. Consequently one of the higher melting GeSP compositions developed by A.R. Hilton<sup>(3)</sup> was prepared and composition development was based on that and the binary GeS system.

Table 1 gives the compositions in the GeGaPS system that were attempted. The GeS<sub>0.5</sub>P composition (Hiltons glass 103) could be prepared at 1000°C, but if the melt temperature was raised to 1100°C explosions resulted even with the thick walled ampoules we used. A DTA of this glass (Figure 4) shows a glass transition temperature at 417°C and a deviation in the baseline at 450°C which suggests a second glass transition that could be due to a second phase. Although the glass is reported to be homogeneous<sup>(3)</sup>, microscopic examination (Figure 5) shows a globular microstructure which is consistent with phase separation. A Knoop hardness of 346±32 (100 g load) was obtained, which is higher than any of the values obtained by Hilton<sup>(3)</sup> (all of Hilton's samples had Knoop hardnesses of ≤250). Reduction of the sulfur content to GeS<sub>0.2</sub>P gave a crystalline material with a high electrical

TABLE 1. GeGaPS COMPOSITIONS PREPARED

Run #	Thermal Expansion, ppm / °C	Comment	Composition			
			Ge	Ga	S	P
1	-		4	2.5	2.5	6
2	-		1	0.6	0.7	1.65
3	-		1.25	1	1	3.75
4	-		1	-	0.5	1
5	-		1	-	0.5	1
6	-		1	-	0.2	1
7	-		1	-	0.5	1
8	-		1	0.33	0.5	1
9	-		1	0.1	0.2	1
10	-		1	0.33	0.5	1
11	11.4		1	0.2	1.5	-
12	-		1	-	1.2	-
13	17.5		1	0.2	2	-
14	-		0.8	0.2	1.5	0.2
15	-		0.8	0.2	2.0	0.2
16	12.1		1	0.4	1.8	-
29	15	Crystal	1	0.2	2.0	-
30	-	Crystal	1	-	2.0	-
31	-	Crystal	1	0.2	2.3	-
32	-	Glass	1	0.2	2.0	-
33	-	Glass	1	-	3.0	-
34	-	Crystal	1	-	2.0	-
35	-	Crystal	1	0.2	2.4	-
36	-	Crystal	1	0.2	2.5	-
37	-	Crystal	1	0.2	2.6	-
38	-	Glass	1	-	4.0	-
39	-	Crystal	1	0.24	2.3	-
40	-	Crystal	1	0.24	2.4	-
41	-	Crystal	1	0.24	2.5	-
42	12	Glass	1	0.24	2.2	0.2
43	17	Glass	1	0.24	2.05	0.2
44	13	Glass	1	0.24	2.05	0.33
45	15	Glass	1	0.24	2.04	0.2
46	-	Crystal	1	0.24	2.3	0.2
47	22	Glass/Crystal	1	0.24	2.0	0.2

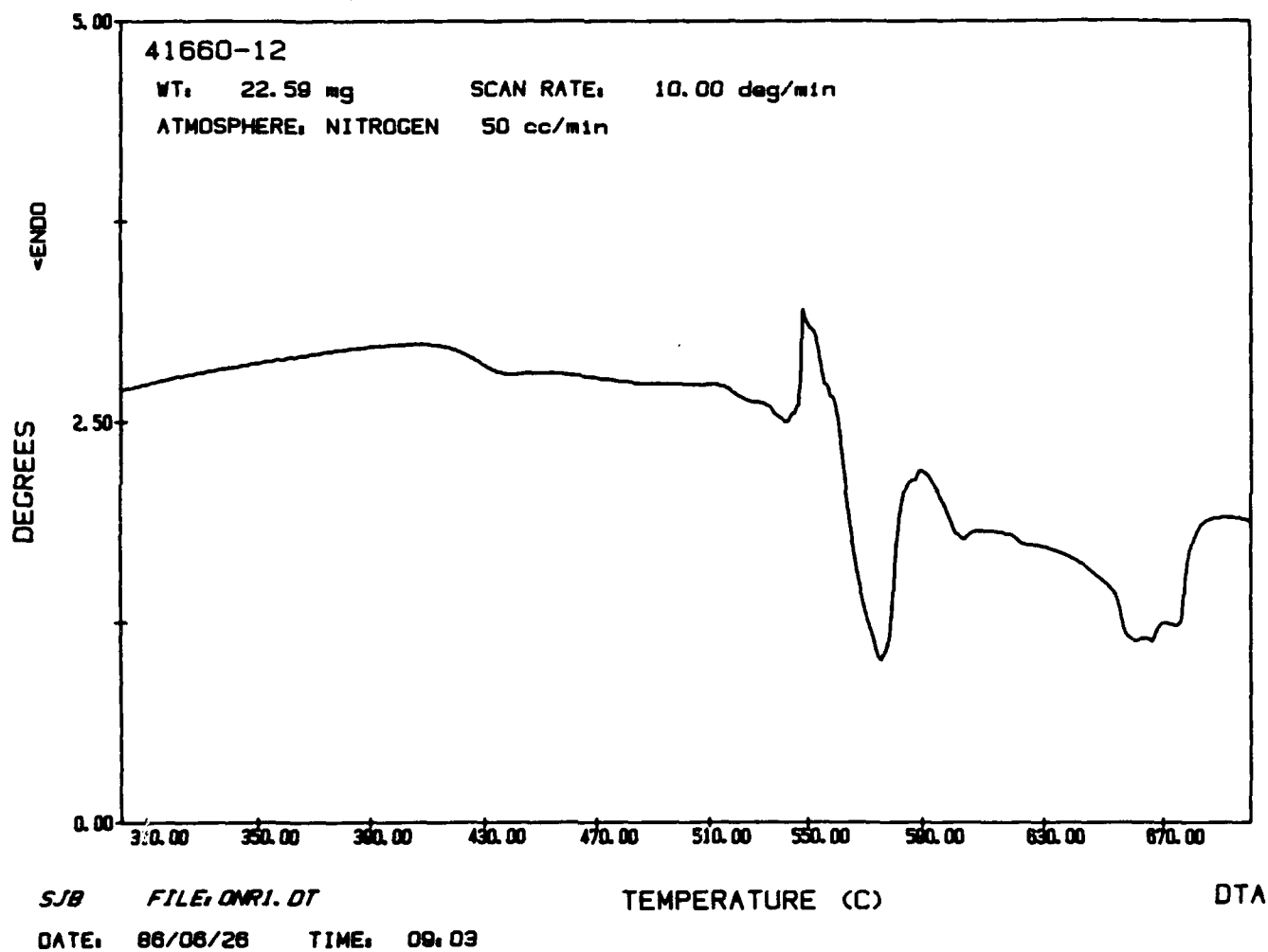
FIGURE 4. DTA OF Ge-S<sub>0.5</sub>P GLASS

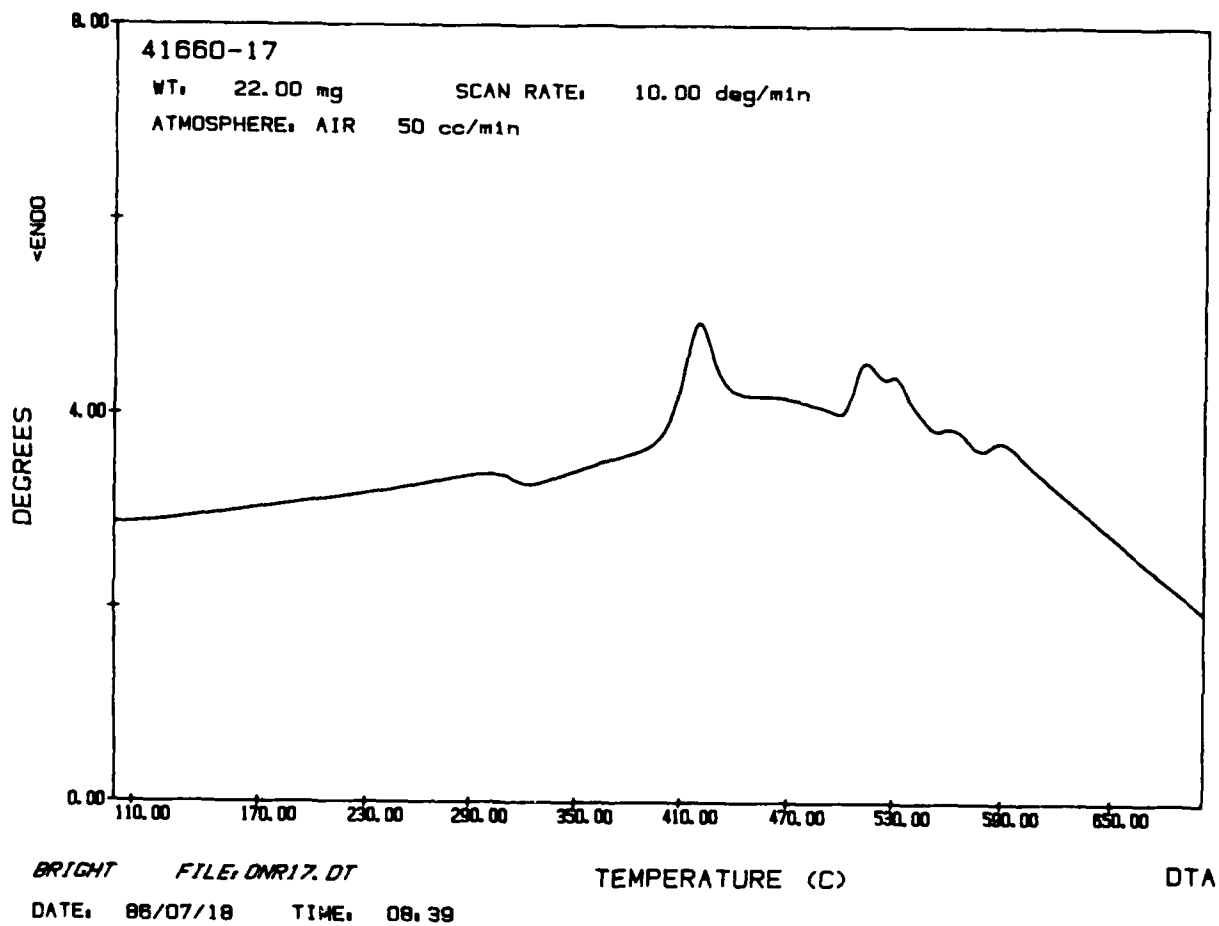


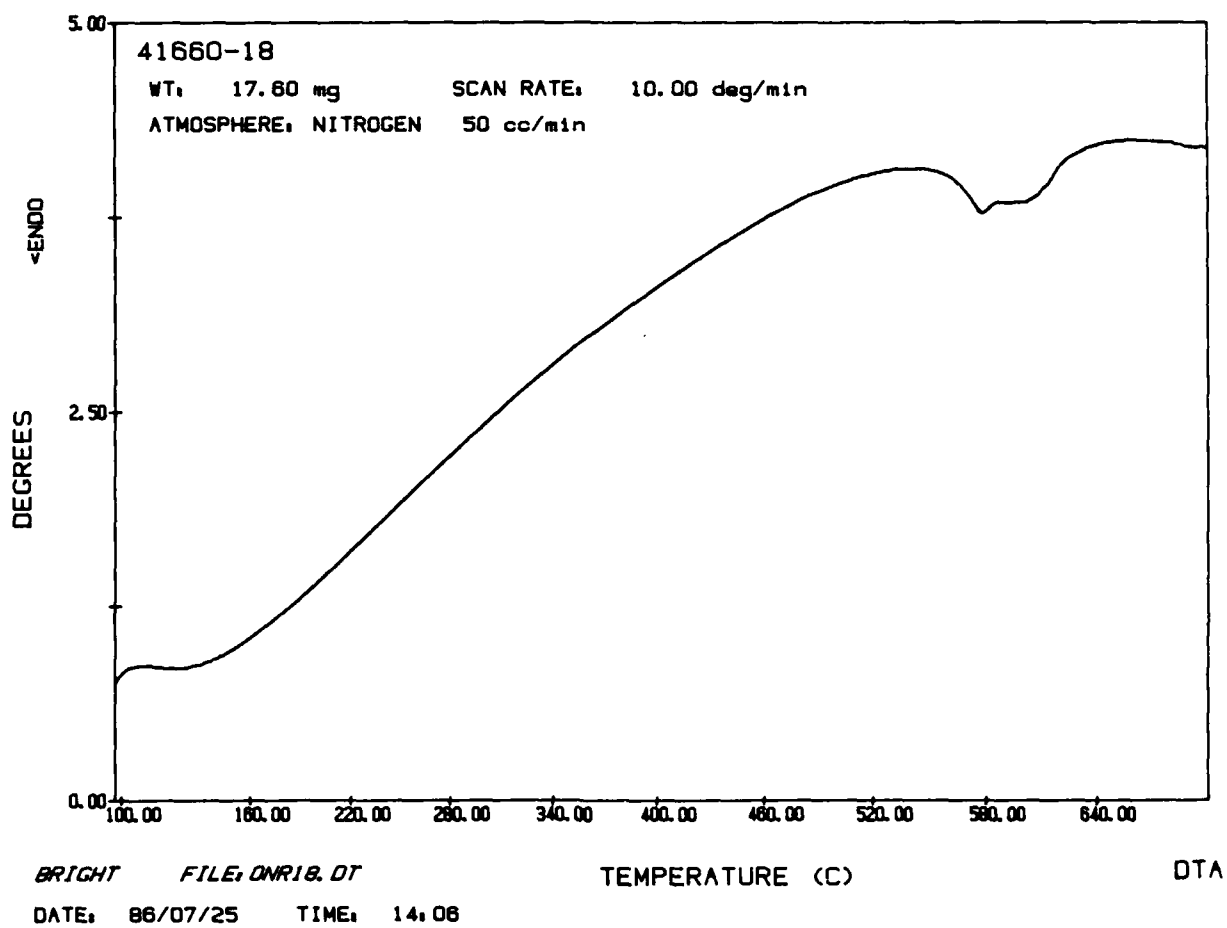
FIGURE 5. GLOBULAR MICROSTRUCTURE OF Ge-S<sub>0.5</sub>P Glass

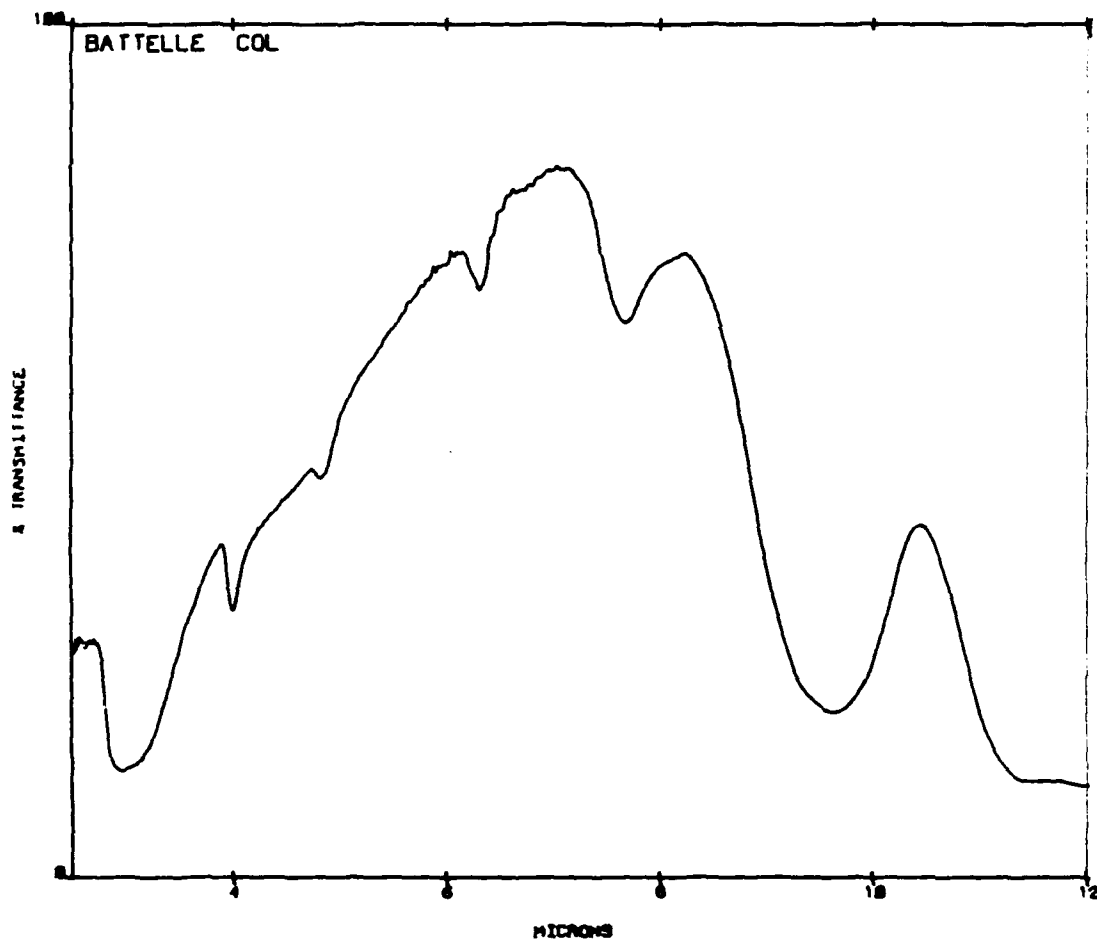
conductivity. Addition of gallium to give the compositions  $\text{GeGa}_{0.33}\text{PS}_{0.5}$  and  $\text{GeGa}_{0.1}\text{PS}_{0.2}$  also gave polycrystalline, electrically conductive materials.

Addition of  $0.2\text{Ga}_2\text{S}_3$  to the  $\text{GeS}_{1.2}$  composition gives a good glass with a glass transition at  $308^\circ\text{C}$ , the first crystallization at  $420^\circ\text{C}$ , and further exotherms at  $530^\circ\text{C}$  (Figure 6). By comparison, the  $\text{GeS}_{1.2}$  glass (Figure 7) does not exhibit any exotherms but has a glass transition at approximately  $570^\circ\text{C}$ . The infrared transmission (Figure 8) shows a large absorption band at  $9.5\ \mu\text{m}$ , the origin of which is uncertain because it is not present in the basic glass. The thermal expansion at  $11\ \text{ppm}/^\circ\text{C}$  is also too high for good thermal-shock resistance. Glass with the composition  $\text{GeGa}_{0.4}\text{S}_{1.8}$  was also prepared and the DTA results are given in Figure 9.

Using powdered germanium from Aldrich as the germanium source, a good, orange-colored, transparent, glass can be prepared with the batch composition  $\text{GeGa}_{0.2}\text{S}_2$ . It has a thermal expansion of  $17.5\ \text{ppm}/^\circ\text{C}$  and the DTA is given in Figure 10. The same composition when prepared with lump germanium is a dark red glass-ceramic with a thermal expansion of  $12.1\ \text{ppm}/^\circ\text{C}$ . The DTA (Figure 11) is significantly different, with a broad exotherm at  $460^\circ\text{C}$  and a sharp endotherm (probably melting) at  $540^\circ\text{C}$ . A possible cause of these difference is the effect of oxygen impurity. The powdered germanium would be expected to have a higher oxygen content than the lump germanium and, even though the ampoules were held at  $10^{-3}$  torr overnight before sealing, surface adsorbed oxygen could still be present. Analytical data are not available for these glasses, but comparison of the oxygen content of the zinc-containing composition  $\text{GeGa}_{0.2}\text{Zn}_{0.1}\text{S}_{2.3}$  (when using the different germanium sources) gives an oxygen content of 2.8 wt% for the powdered germanium and 1.2 wt.% for the lump germanium. This points out a need for the monitoring of oxygen contents in sulfide glasses, something which is not normally done in the field. Even 1.2 percent is a high level, so the decision was made to develop the pressure furnace so that melts could be prepared in an environment where the melt was not in contact with an oxide container. Further melts were also prepared in the GeS and GeGaS systems and DTA's of the  $\text{GeS}_3$  and  $\text{GeS}_4$  glasses are given in Figures 12 and 13. The other batches produced crystalline products that were mechanically very weak and so were not evaluated further.

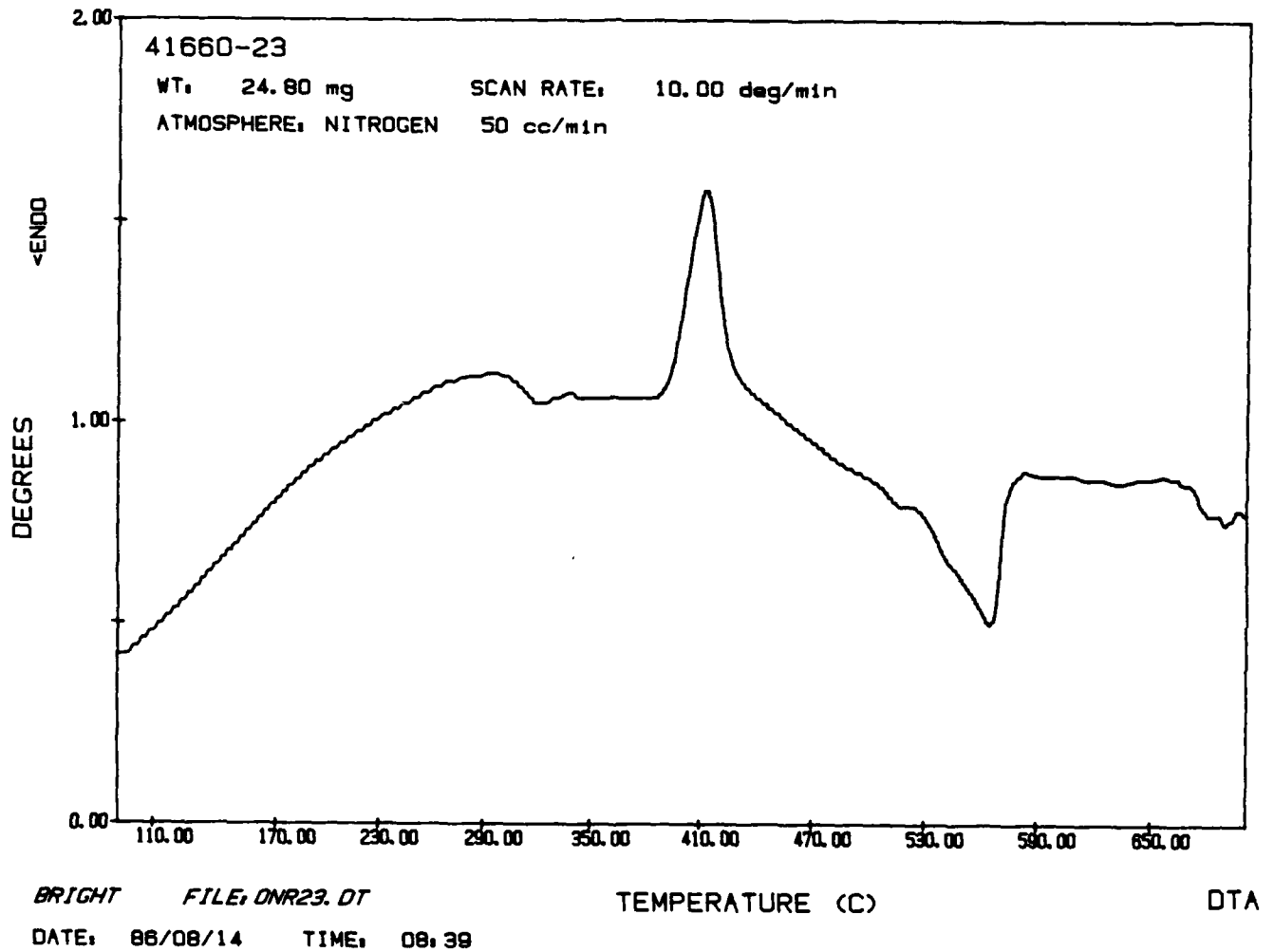
FIGURE 6. DTA OF 0.1 Ga<sub>2</sub>S<sub>3</sub>-GeS<sub>1.2</sub>

FIGURE 7. DTA OF GeS<sub>1.2</sub> GLASS



PFA-R4166X17A  
NSCANS=200  
FCT=AL

FIGURE 8. INFRARED TRANSMISSION SCAN OF  $\text{GeGa}_{0.2}\text{S}_{1.5}$

FIGURE 9. DTA OF GeGa<sub>0.4</sub>S<sub>1.8</sub> GLASS

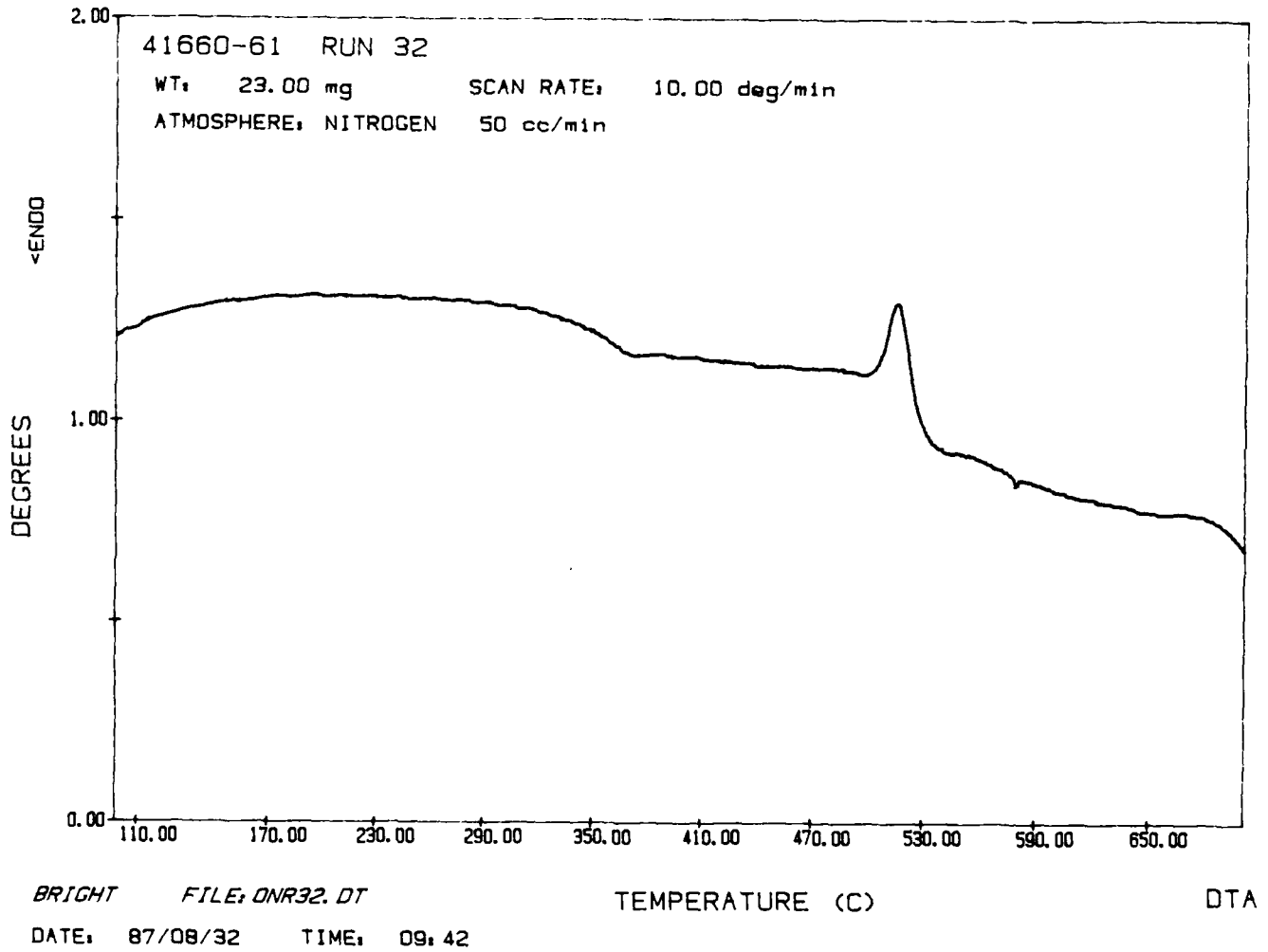


FIGURE 10. DTA OF  $\text{GeGa}_{0.2}\text{S}_2$  GLASS USING POWDERED GERMANIUM

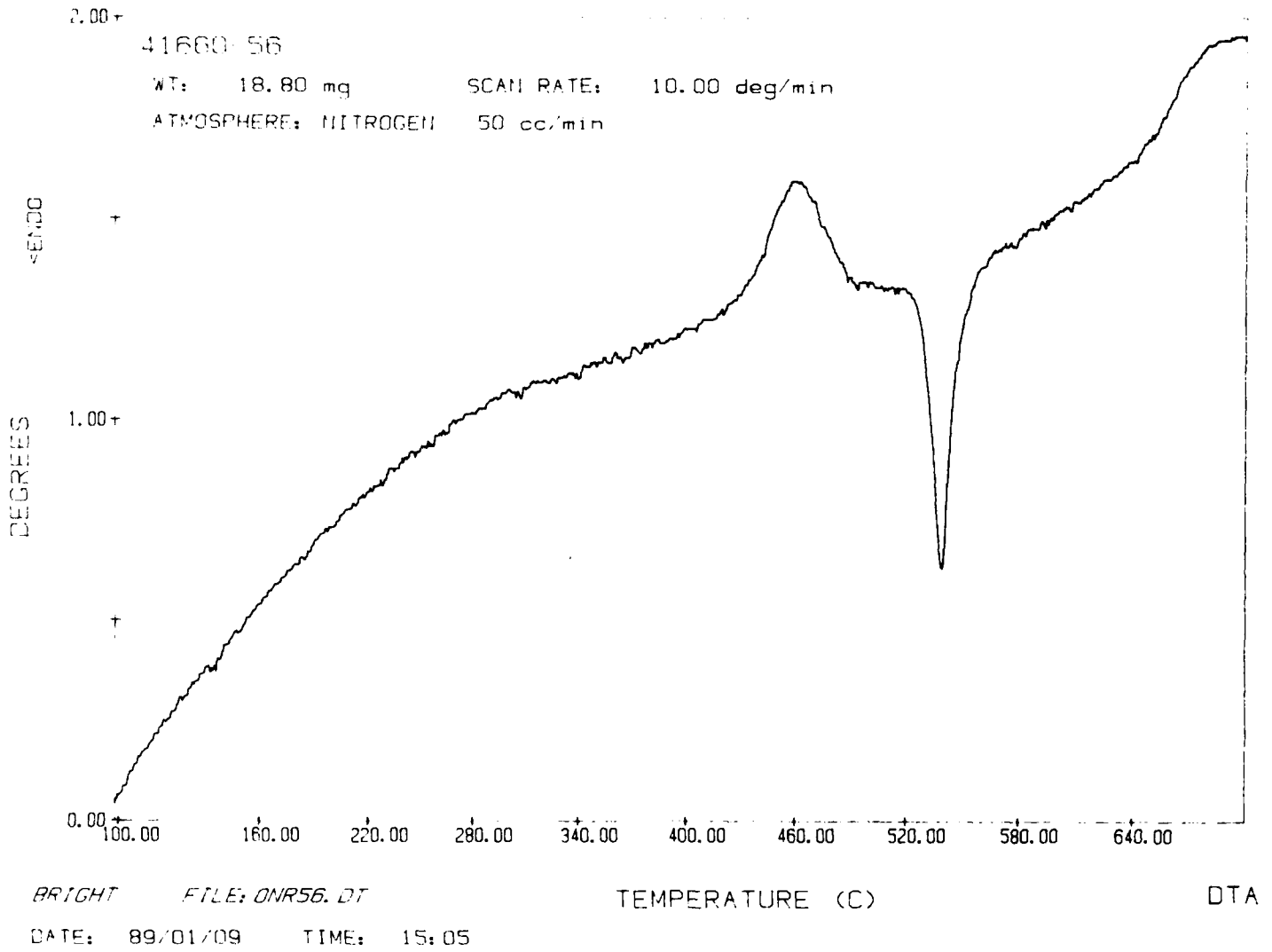
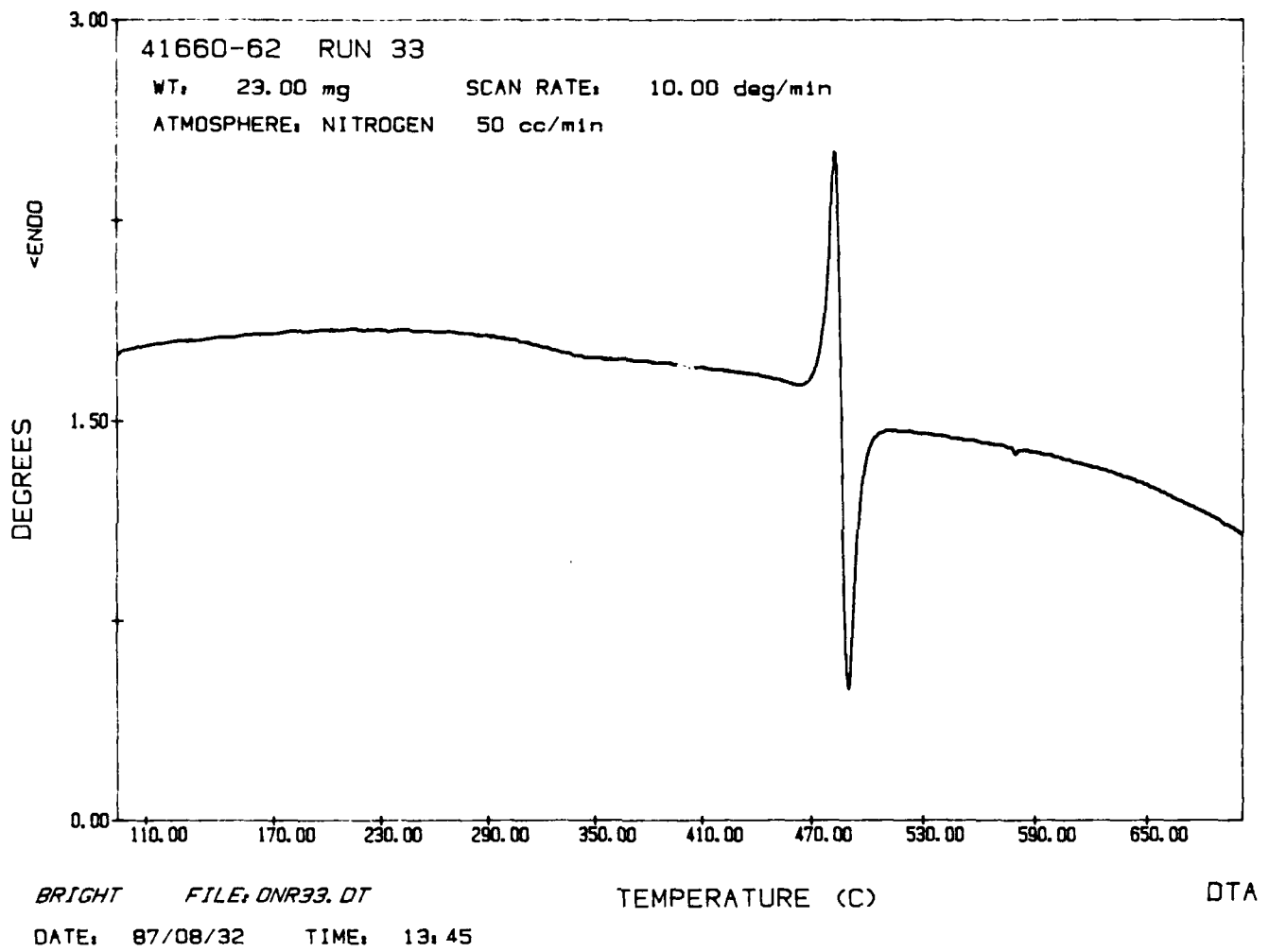
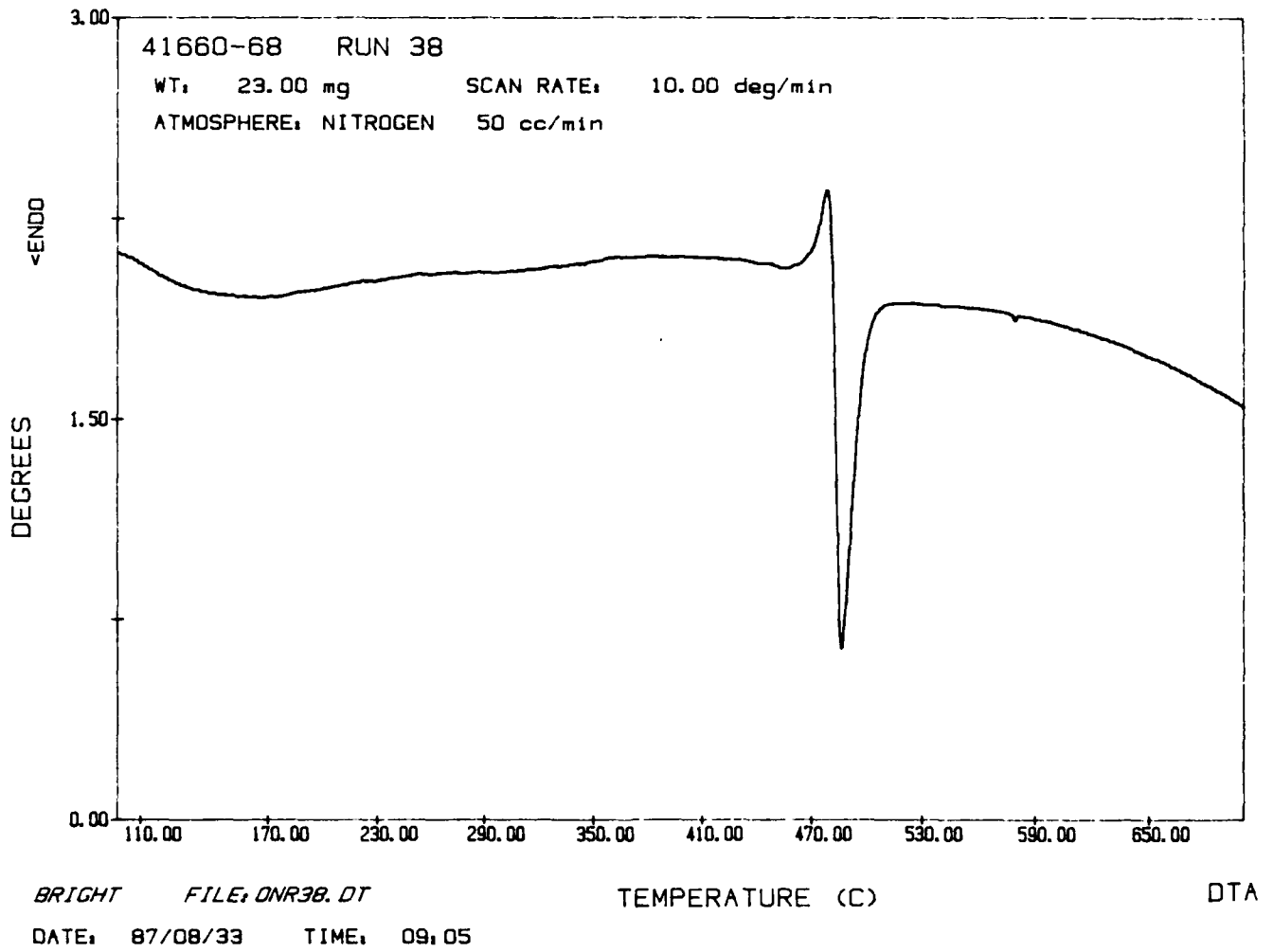


FIGURE 11. DTA OF  $\text{GeGa}_{0.2}\text{S}_2$  GLASS USING LUMP GERMANIUM

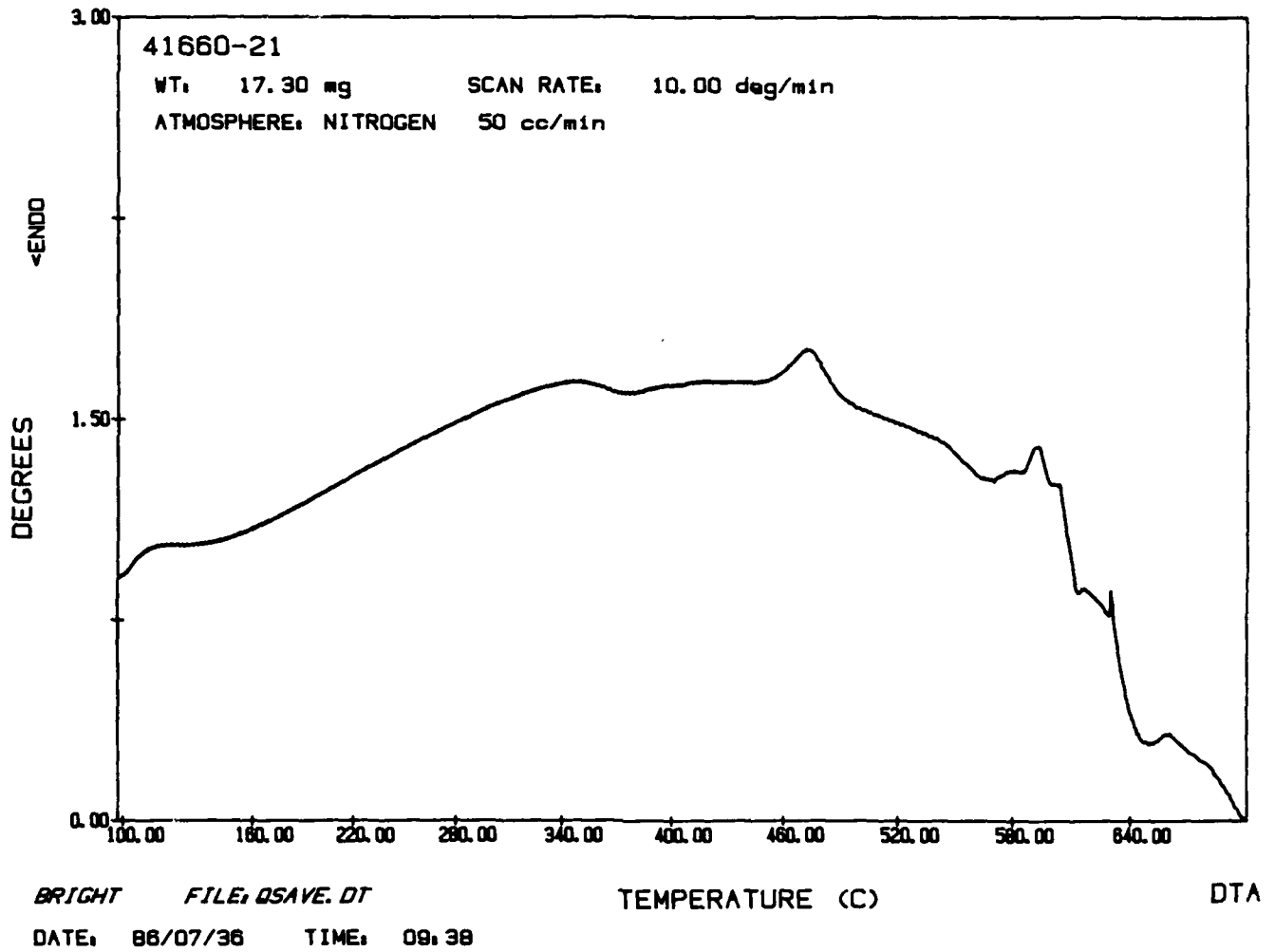
FIGURE 12. DTA OF GeS<sub>3</sub> GLASS

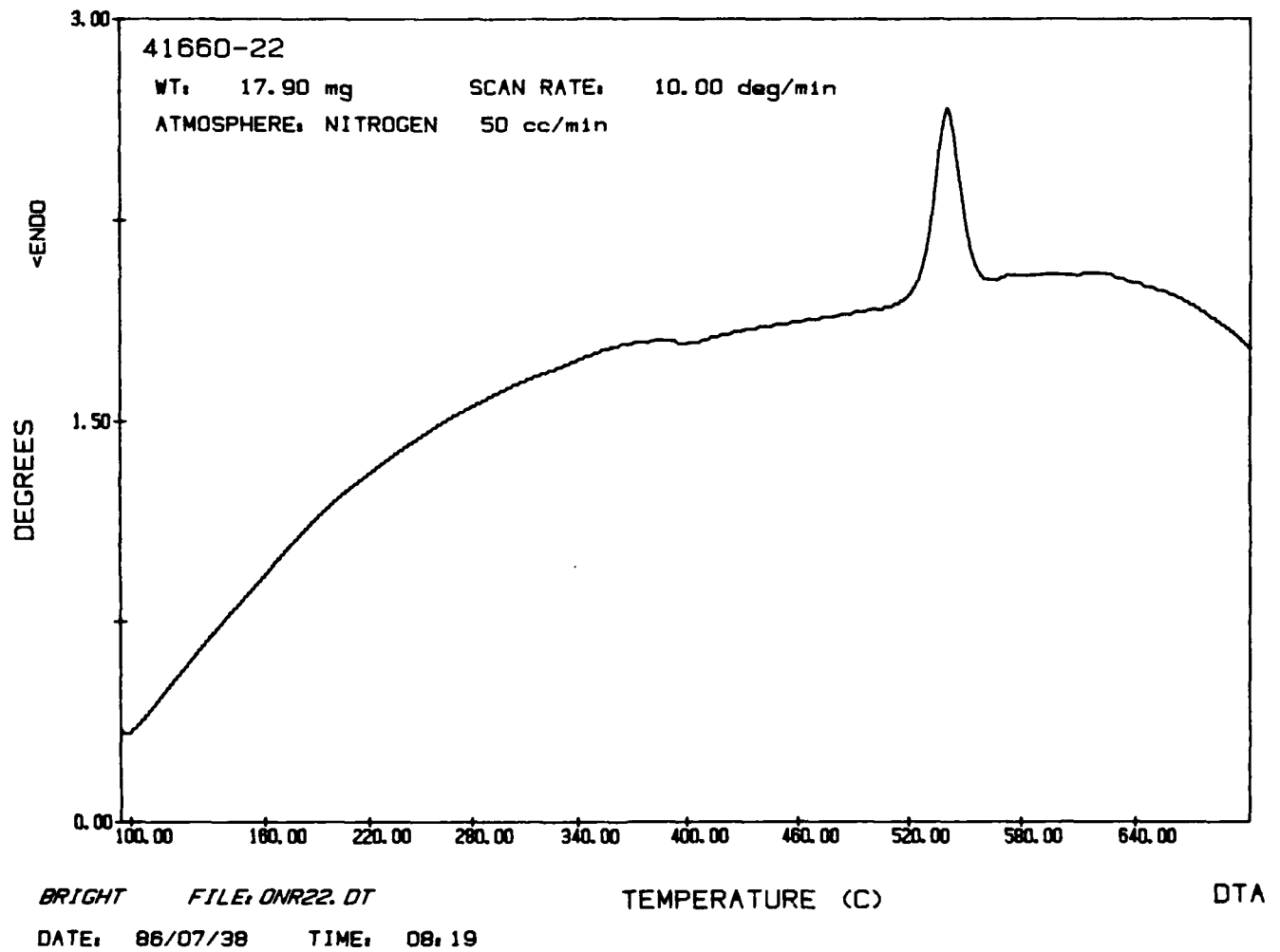
FIGURE 13. DTA OF GeS<sub>4</sub> GLASS

Based upon the  $\text{GeGa}_{0.2}\text{S}_2$  glass, a series of phosphorus-containing materials were prepared. DTA's of the first two compositions are given in Figures 14 and 15. The  $\text{GeGa}_{0.25}\text{P}_{0.25}\text{S}_{1.88}$  sample was electrically conductive and so was not further studied. However the addition of small amounts of sulfur and variation of the phosphorus content gave a series of glasses with thermal expansions between 12 and 17 ppm/°C. In the high-sulfur glass (Figure 16) there are two exothermic peaks, a broad peak at approximately 500°C and a distinct crystallization peak at approximately 600°C. In both of the lower-sulfur samples (Figure 17) the second large exotherm is absent.

### Crystallization Studies

The composition  $\text{GeGa}_{0.24}\text{P}_{0.2}\text{S}_2$  forms a good glass when melted in the pressure furnace. It was prepared by slow heating (5°C/min) to 1050°C, holding for 4 hrs., then rapid cooling to room temperature under an argon pressure of 1500-3000 psi (depending upon the temperature). The DTA (Figure 18) shows a glass transition at 360°C and an exotherm at 460°C. The thermal expansion is 13 ppm/°C. A detailed study of the crystallization behavior of this glass has been conducted in order to determine which crystalline phases will naturally form from the GeGaPS system. X-ray diffraction was not found to be useful so the work concentrated on the microstructural examination of polished sections in an electron microprobe. A sample of the glass which had been slow-cooled and partially crystallized was closely examined. Figure 19 is a typical crystal. Quantitative wavelength-dispersive X-ray analysis of the crystal showed it to be  $\text{GeGa}_{0.05}\text{S}_{1.32}$  with no phosphorus present. This is effectively a slightly doped germanium sulfide. In the bulk, the measured composition was  $\text{GeGa}_{0.24}\text{P}_{0.03}\text{S}_{2.03}$  which, except for some phosphorus loss, is close to the batch composition. Under normal secondary electron imaging no further detail was observed. However if the sample is imaged in back-scattered-electron mode and the accelerating voltage is carefully controlled, then a detailed microstructure is revealed (Figure 20). Zoned mixed crystals of a germanium-gallium sulfide with a gallium sulfide core are present (Figure 21, dark areas) and regions of a "wheat sheaf" morphology (Figure 22) are

FIGURE 14. DTA OF  $\text{GeGa}_{0.25}\text{P}_{0.25}\text{S}_{1.88}$

FIGURE 15. GeGa<sub>0.25</sub>S<sub>2.5</sub>P<sub>0.25</sub> GLASS

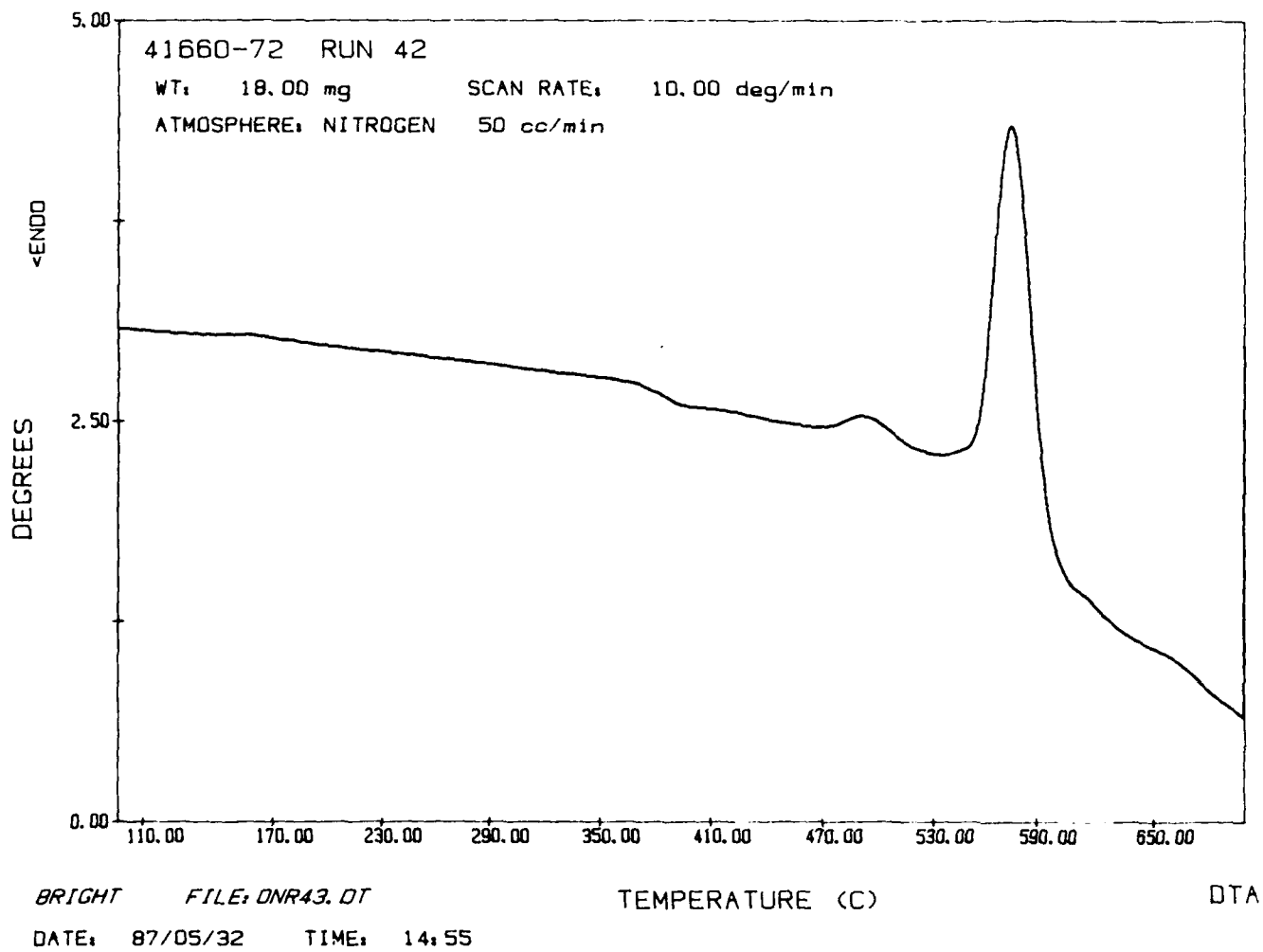


FIGURE 16. DTA OF HIGH SULFUR GLASS

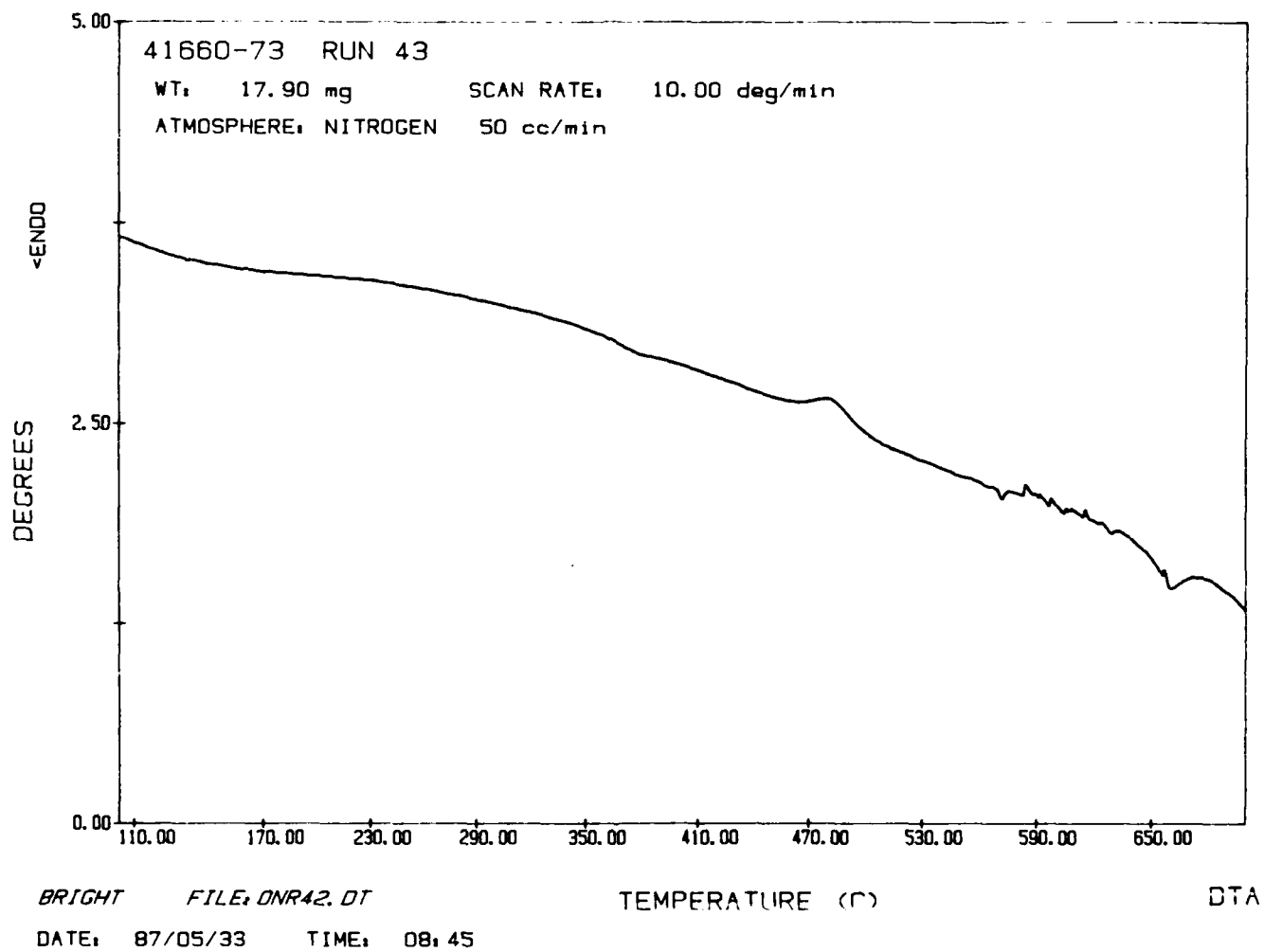


FIGURE 17. DTA OF LOW SULFUR GLASS

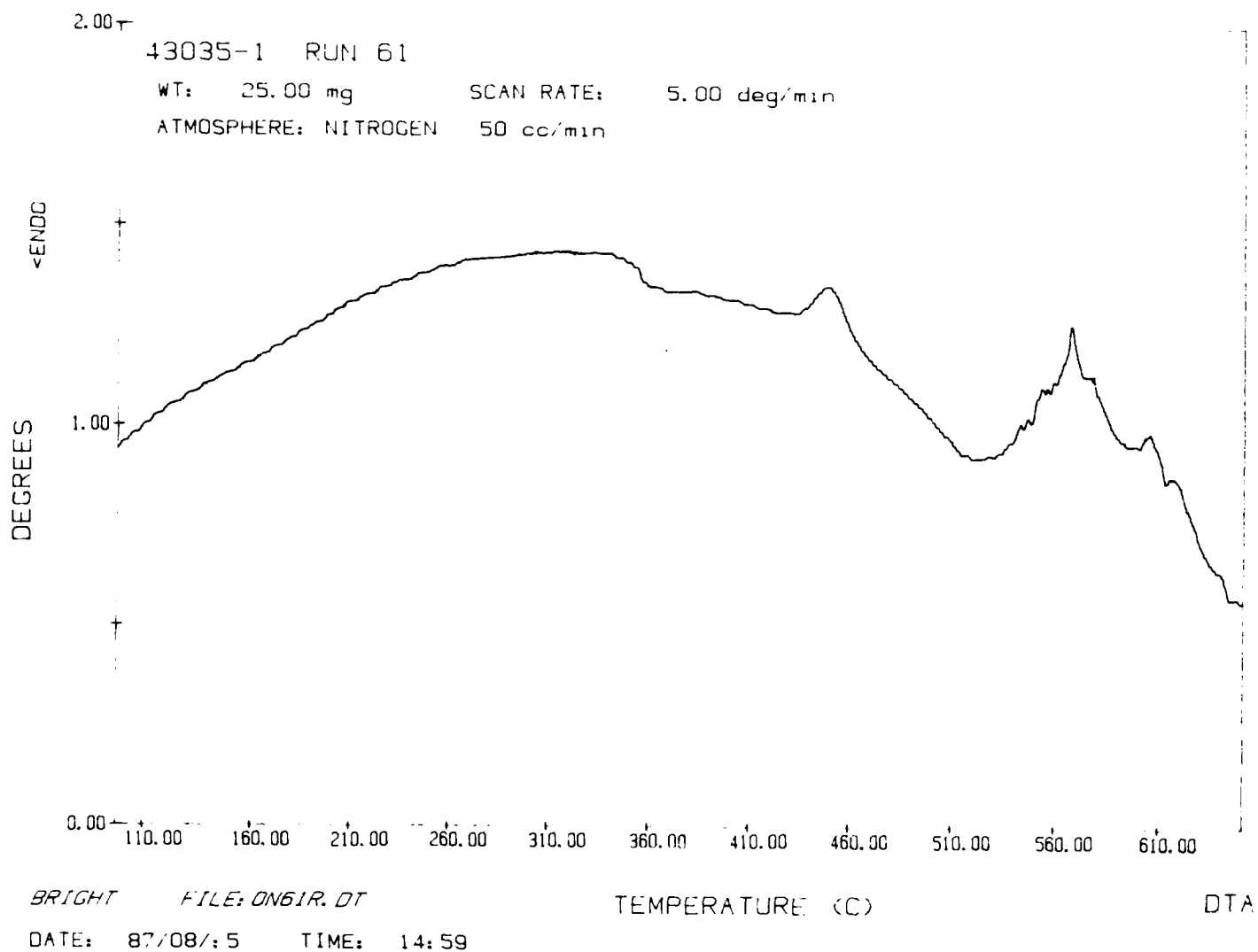


FIGURE 18. DTA OF  $\text{GeGa}_{0.24}\text{P}_{0.2}\text{S}_2$  GLASS  
MELTED IN THE PRESSURE FURNACE



FIGURE 19. TYPICAL CRYSTAL OF GeGaPS GLASS



FIGURE 20. MICROSTRUCTURE OF GeGaPS GLASS

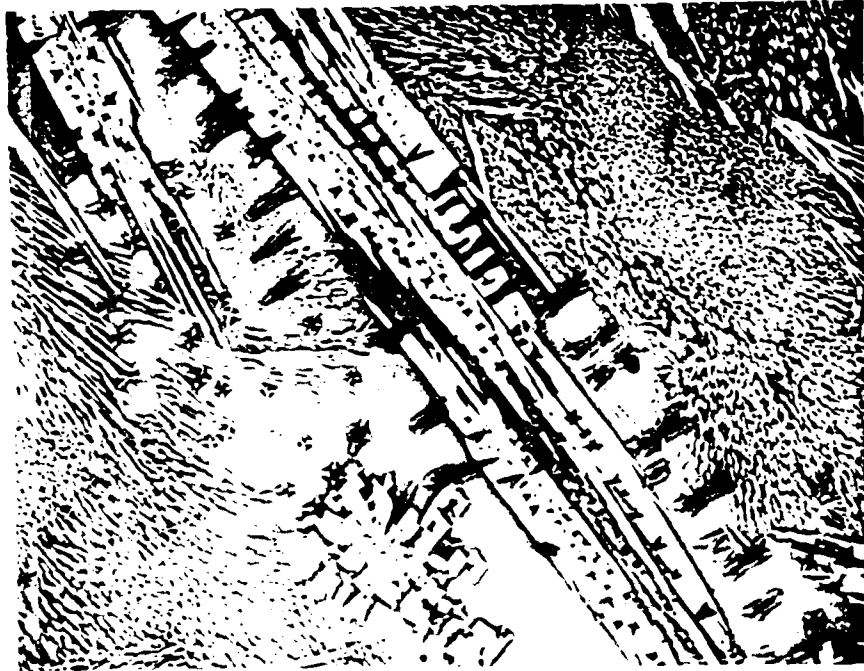


FIGURE 21. ZONED MIXED CRYSTALS



FIGURE 22. "WHEAT SHEAF" MORPHOLOGY

present. The small dimensions of the "wheat sheaf" crystals prevent an accurate analysis of their composition however.

In order to study the crystallization of  $\text{GeGa}_{0.24}\text{P}_{0.2}\text{S}_2$  in more detail a series of glass samples were annealed under the conditions described in Table 2.

TABLE 2. ANNEALING TREATMENTS FOR GeGaPS GLASSES

Time (hrs)	0	2	4	8	16	32	64
Temperature (°C)							
Unannealed	*						
450			*	*	*		
500		*	*	*	*		
550			*	*	*		
600		*	*	*	*	*	*

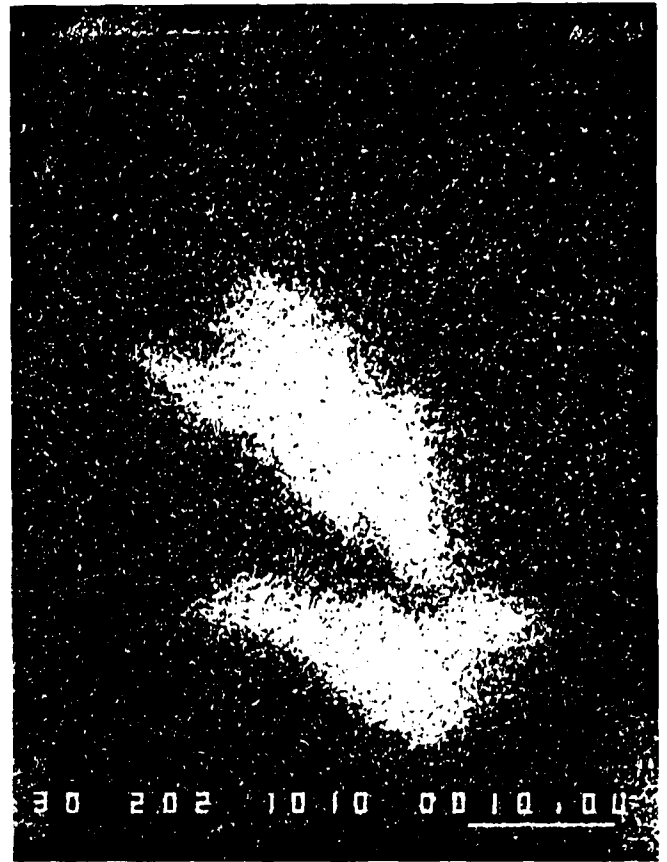
There were some needle-like gallium sulfide crystals (Figure 23) present in zones in the unannealed glass that are probably the result of vapor-grown crystals falling into the melt from the lid of the crucible where they form. Despite the large exotherm in the DTA at 460°C, none of the anneals at 450°C nor the two-hour anneal at 500°C had any effect on the microstructure. At four and eight hours (500°C) 1- $\mu\text{m}$  "blocky" crystals appear in the regions free from needle-like crystals (Figure 24). At 16 hours (500°C) the "blocky" crystals are uniformly distributed in the glass. Because of their small size, analysis of their composition in the microprobe is not possible. At 550°C the results were similar to what was found at 500°C. The 2-hour, 4-hour and 8-hour anneals at 600°C gave the same "blocky" crystals as at 500°C but at eight hours large (20-200  $\mu\text{m}$ ) crystals are also present (Figure 25). Elemental analysis (WDS) of a typical large crystal (Table 3) shows a gallium sulfide crystal with a mixed germanium-gallium sulfide surface.



FIGURE 23. NEEDLE LIKE GALLIUM SULFIDE CRYSTALS



FIGURE 24. "BLOCKY" CRYSTALS



Gallium Map

FIGURE 25. LARGE CRYSTALS - 8 HOUR ANNEAL

TABLE 3. ANALYSIS OF LARGE CRYSTALS FORMED AT 600°C (8 hrs.)

Crystal Core	Crystal Outer Edge	Matrix
Ge - 0.03 (wt.%)	Ge - 14.07 (wt.%)	Ge - 34.26 (wt.%)
Ga - 37.25 (wt.%)	Ga - 25.07 (wt.%)	Ga - 4.66 (wt.%)
P - 0.00 (wt.%)	P - 1.67 (wt.%)	P - 5.96 (wt.%)
S - 62.71 (wt.%)	S - 59.19 (wt.%)	S - 56.82 (wt.%)

The compositional gradient at the glass/crystal interface is shown in Figure 26. At 16 hours (600°C) a rich morphology develops. The small "blocky" crystals and the large gallium sulfide crystals observed at 8 hours are still present but, in addition, extensive large arrays of "wheatsheaf" crystals are observed and large black contrast regions/crystals that are sulfur-rich and phosphorus-depleted are found. In the 32 and 64 hour samples (600°C) the needle-like crystals and the small blocky crystals have disappeared. There are extensive rectangular crystals (Figure 27) 2-15  $\mu\text{m}$  across that are probably germanium sulfides (by EDX analysis), and there are extensive dark-contrast crystals (30-150  $\mu\text{m}$  in length) that are gallium-depleted and sulfur-rich. Light grey contrast crystals similar to those observed at 16 hours are also observed.

#### Nuclear Magnetic Resonance Studies

Questions were raised about whether the phosphorus was going into the reduced ( $\text{P}^-$ ) state, so we decided to do some preliminary  $^{31}\text{P}$  NMR work to examine this question. NMR chemical shifts are sensitive to the electron density at the nucleus, so solid state spectra are dependant both on the charge on the phosphorus and on the coordination number (which influences orbital hybridization). Five compositions were measured (Figures 28-32) and the results are summarized in Table 4. Phosphoric acid is the standard at zero chemical shift so the large broad peaks at zero in some of the spectra indicate that phosphate impurities are present.

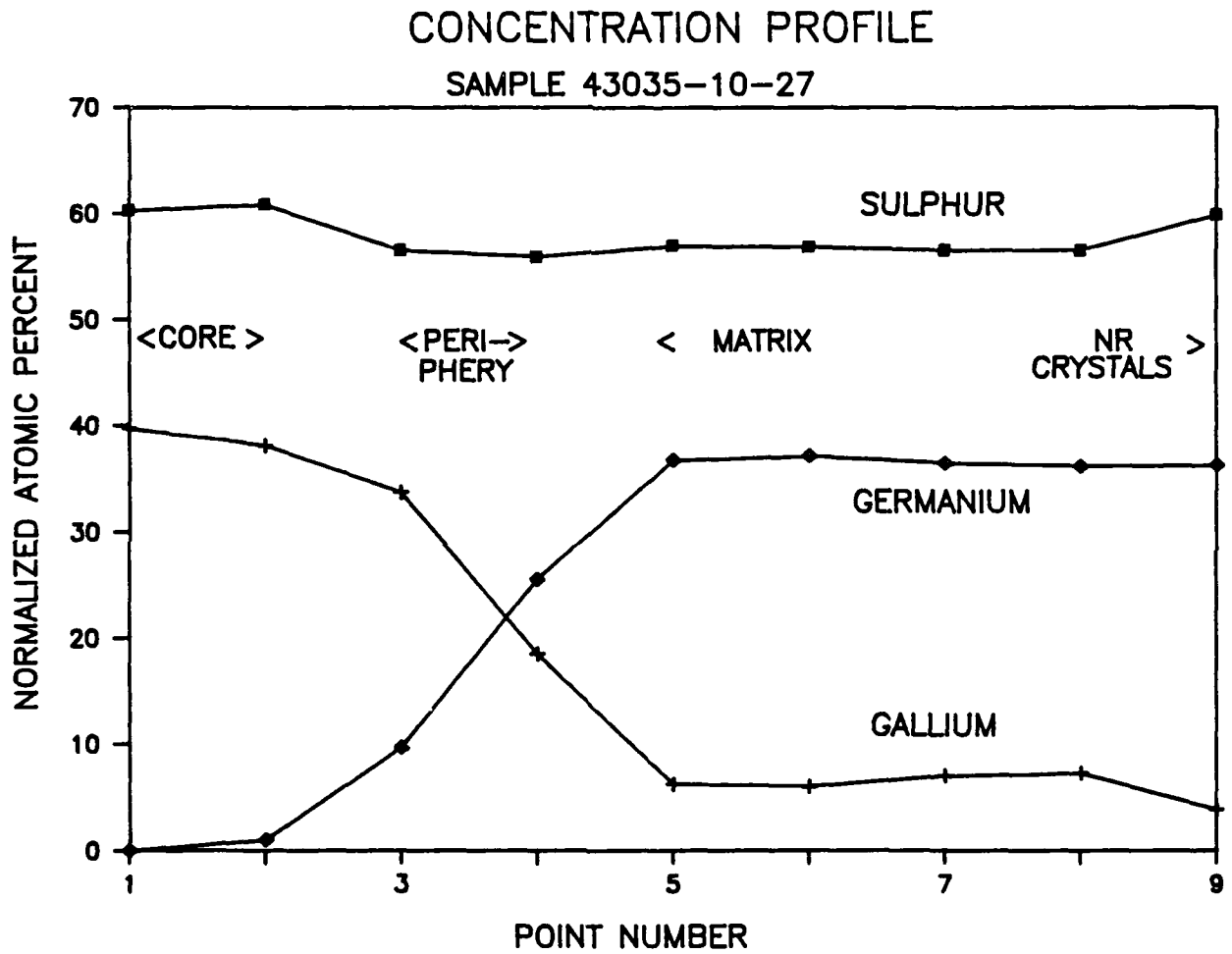


FIGURE 26. CONCENTRATION PROFILE AT THE GLASS-CRYSTAL INTERFACE

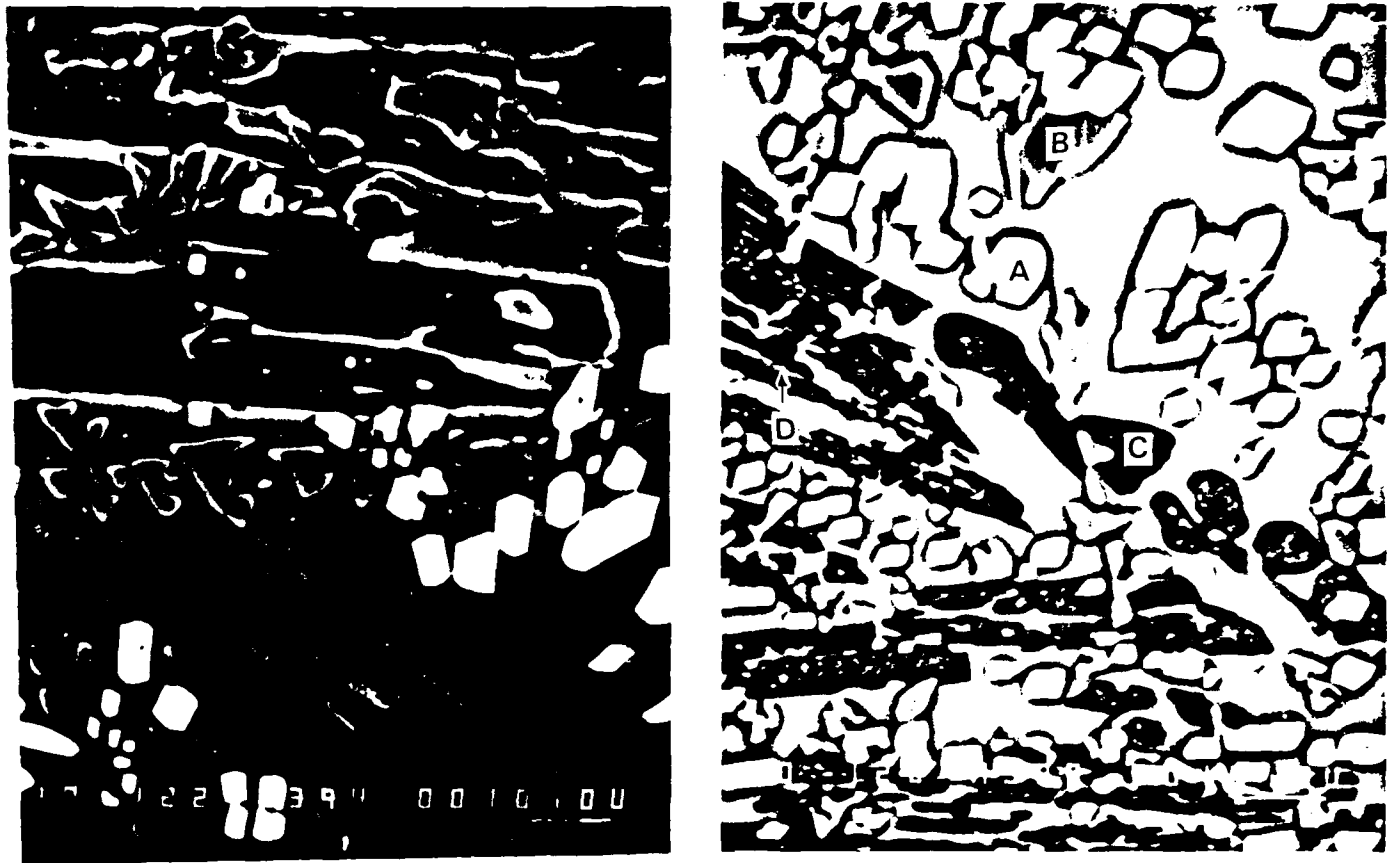


FIGURE 27. MICROSTRUCTURE OF  $\text{GeGa}_{24}\text{P}_{0.2}\text{S}$  AFTER 64 HOURS AT 600 C

TABLE 4. SUMMARY OF  $^{31}\text{P}$  NMR RESULTS

Batch Ge	Composition Ga	P	S	Comments	Morphology
1	0.33	1	0.5	Phosphate, Broad with Spikes	Crystals
0.8	0.2	0.2	2.0	+ ve Phosphorous Many Sharp Lines	Glass
1	0.133	1	0.2	Phosphate, Broad with Spikes (Reduced)	Glass Ceramic
1	-	1	0.5	No Phosphate, Amorphous (Reduced P)	Glass
1	-	1	0.2	Phosphate, Broad with Spikes (Reduced)	Crystals

From these data we can conclude that NMR is a good indicator of phosphate impurity levels, which is important because phosphate absorbs in the 8-12  $\mu\text{m}$  region. We can also conclude that phosphorus is usually in the reduced state in these materials. A qualitative view of the crystallinity of the sample can also be obtained by examining the sharpness and multiple line features in the spectrum.

#### Ge-Ga-Zn-S-P and Ge-Zr-S Systems

The GeGaZnSP system was studied to evaluate its potential for forming glass-ceramics. The addition of Zinc has the added advantage that Zinc is strongly electropositive and so will force the Phosphorus into a reduced state. Table 5 gives the compositions studied and the thermal expansions found. The DTA for  $\text{GeZn}_{0.1}\text{Ga}_{0.2}\text{S}_{2.3}$  did not display any features up to 700°C, so it is most likely fully crystalline. Changing the germanium source from

Ge Ga<sub>0.33</sub> P S<sub>0.5</sub>

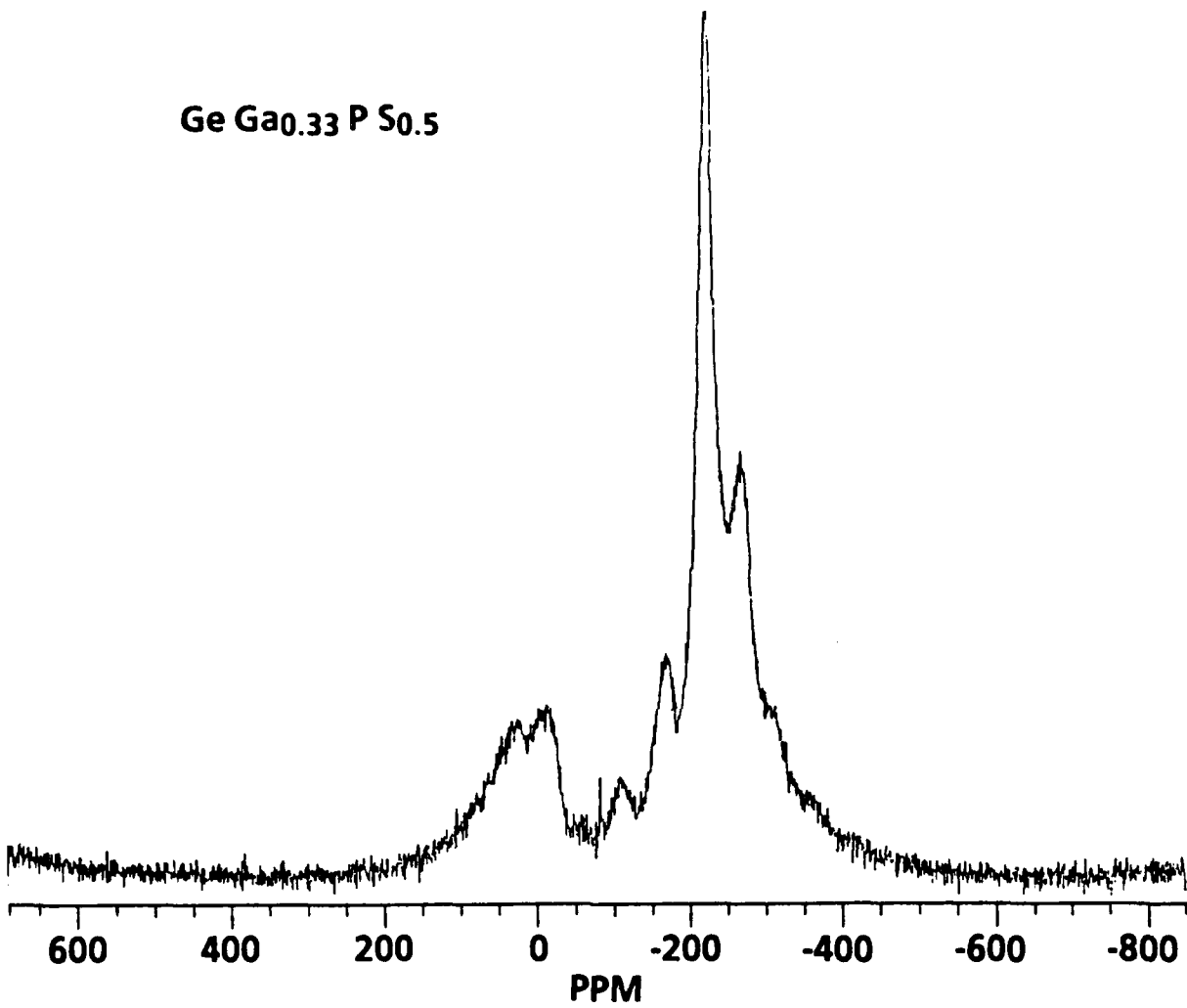


FIGURE 28. NMR SPECTRUM OF GeGa<sub>0.33</sub>P<sub>0.5</sub>

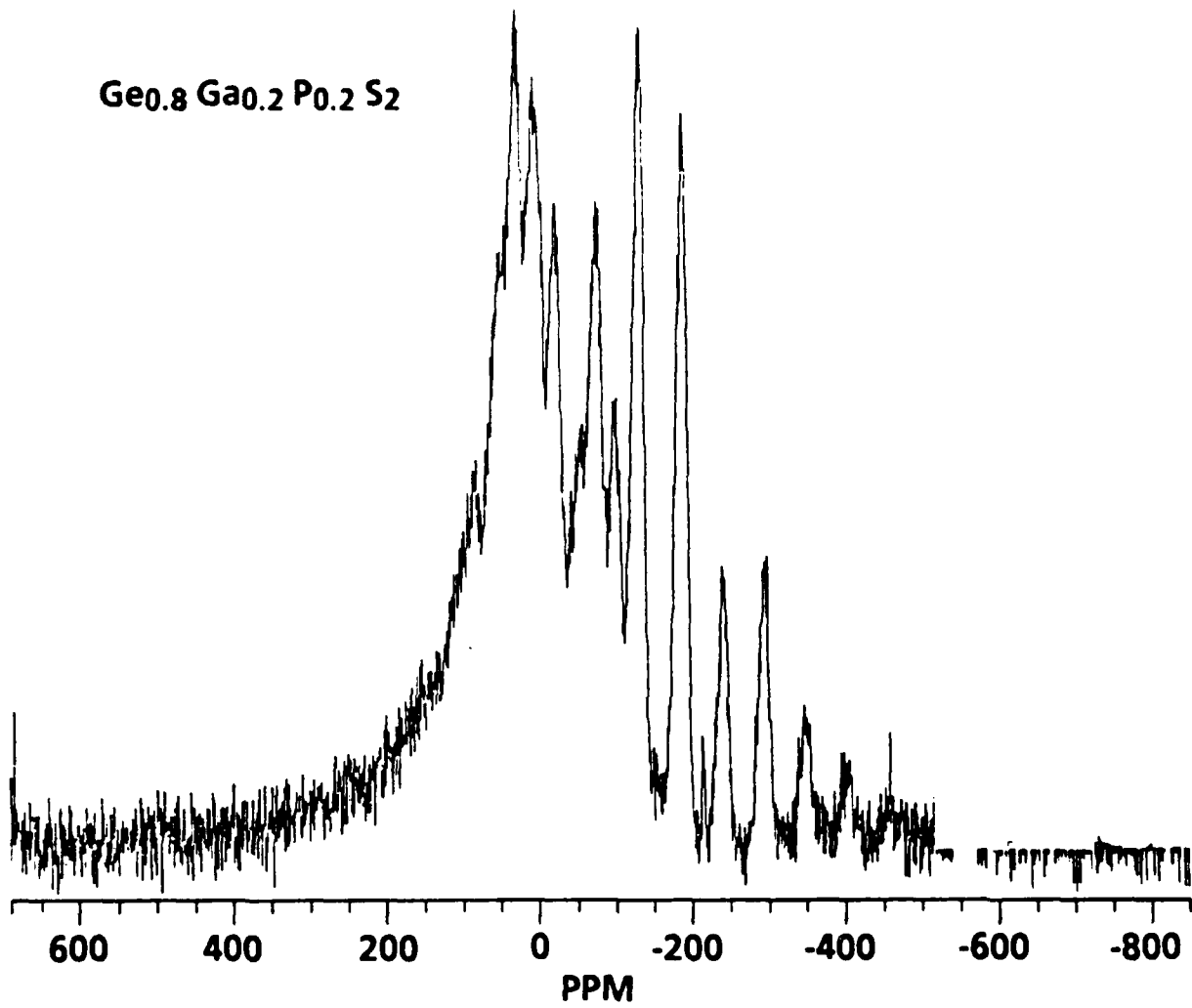


FIGURE 29. NMR SPECTRUM OF  $\text{GeGa}_{.25}\text{P}_{.25}\text{S}_{2.5}$

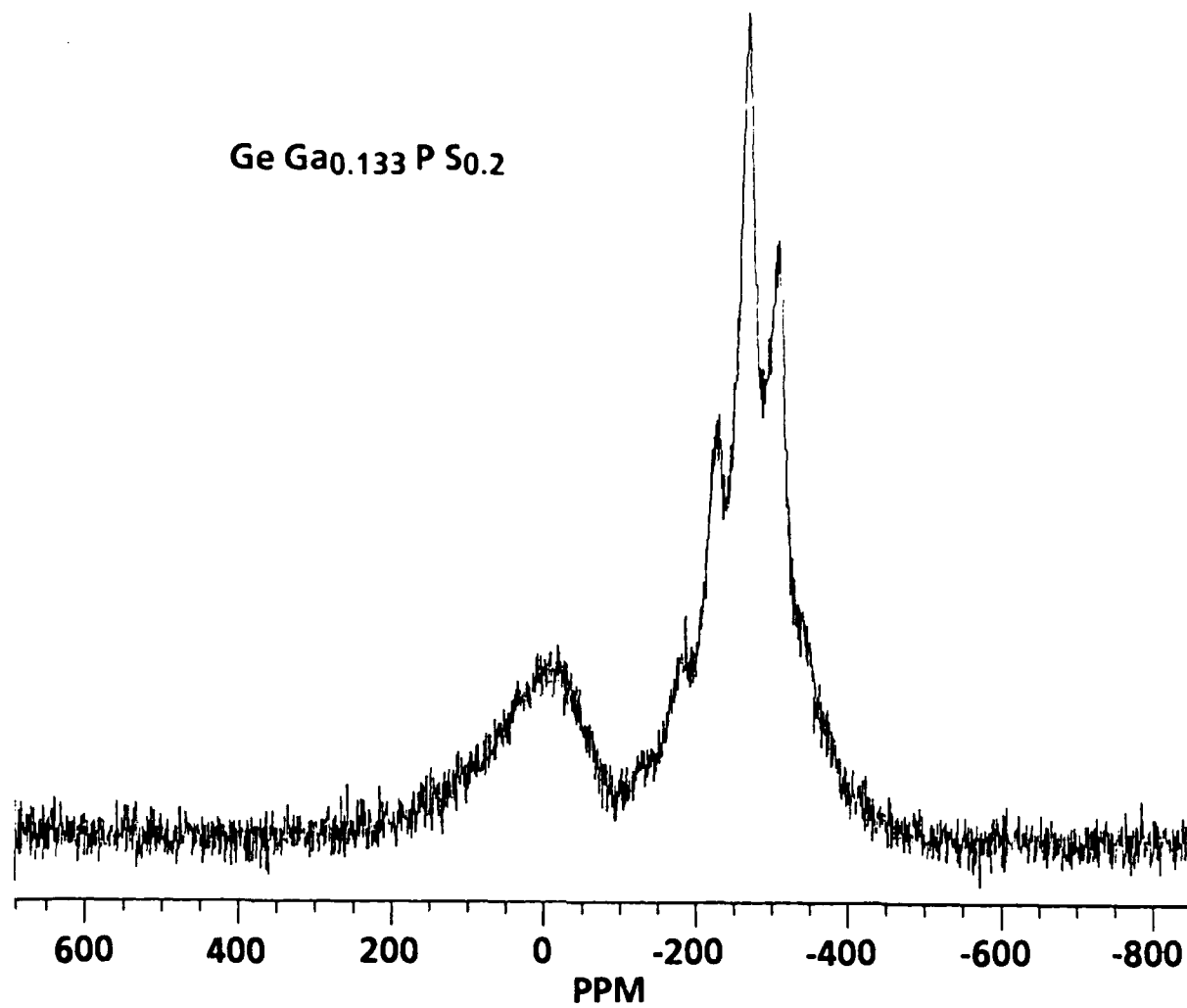


FIGURE 30. NMR SPECTRUM OF GeGa<sub>0.133</sub>PS<sub>0.2</sub>

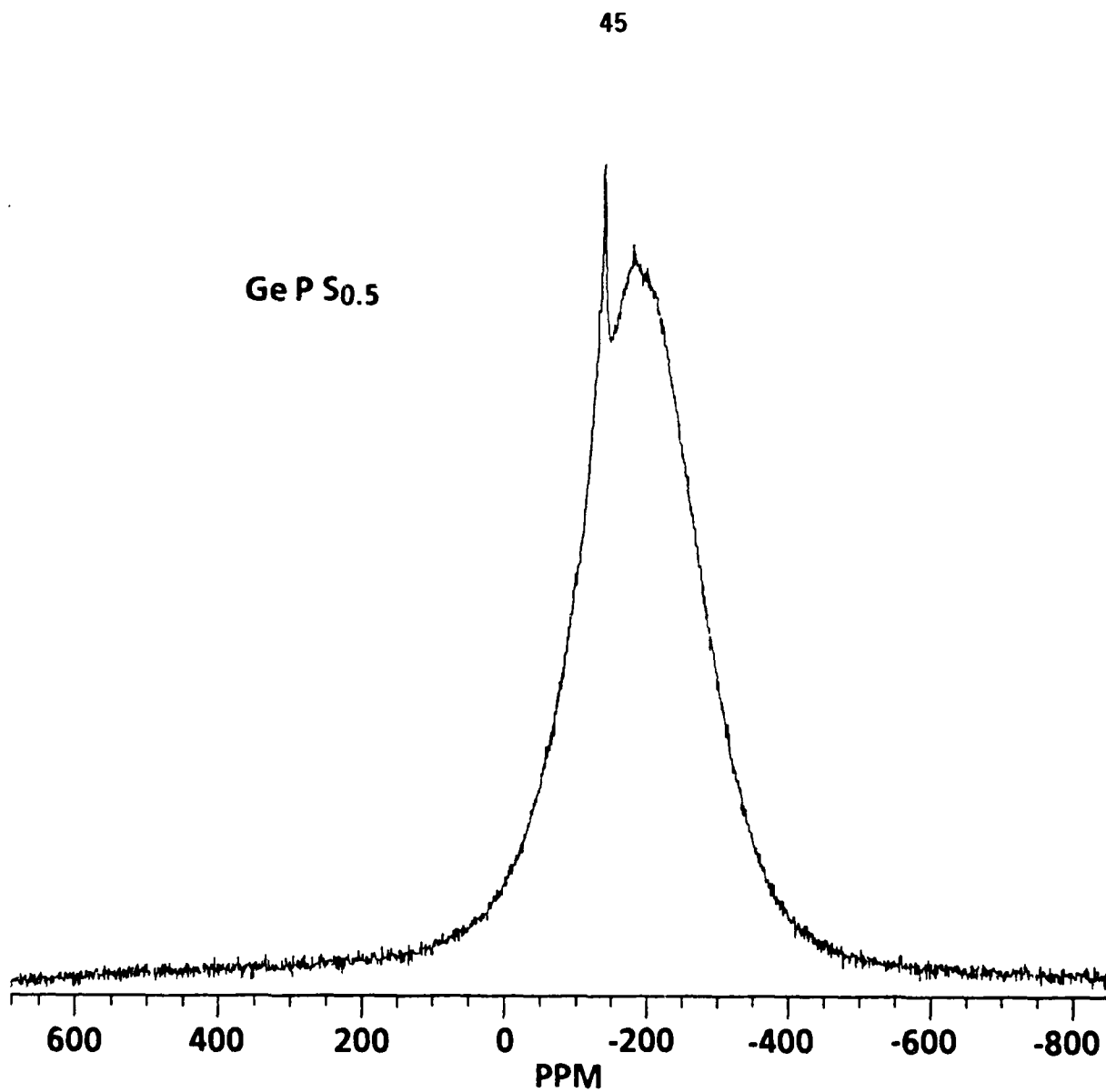


FIGURE 31. NMR SPECTRUM OF GePS<sub>0.5</sub>

Ge P S<sub>0.2</sub>

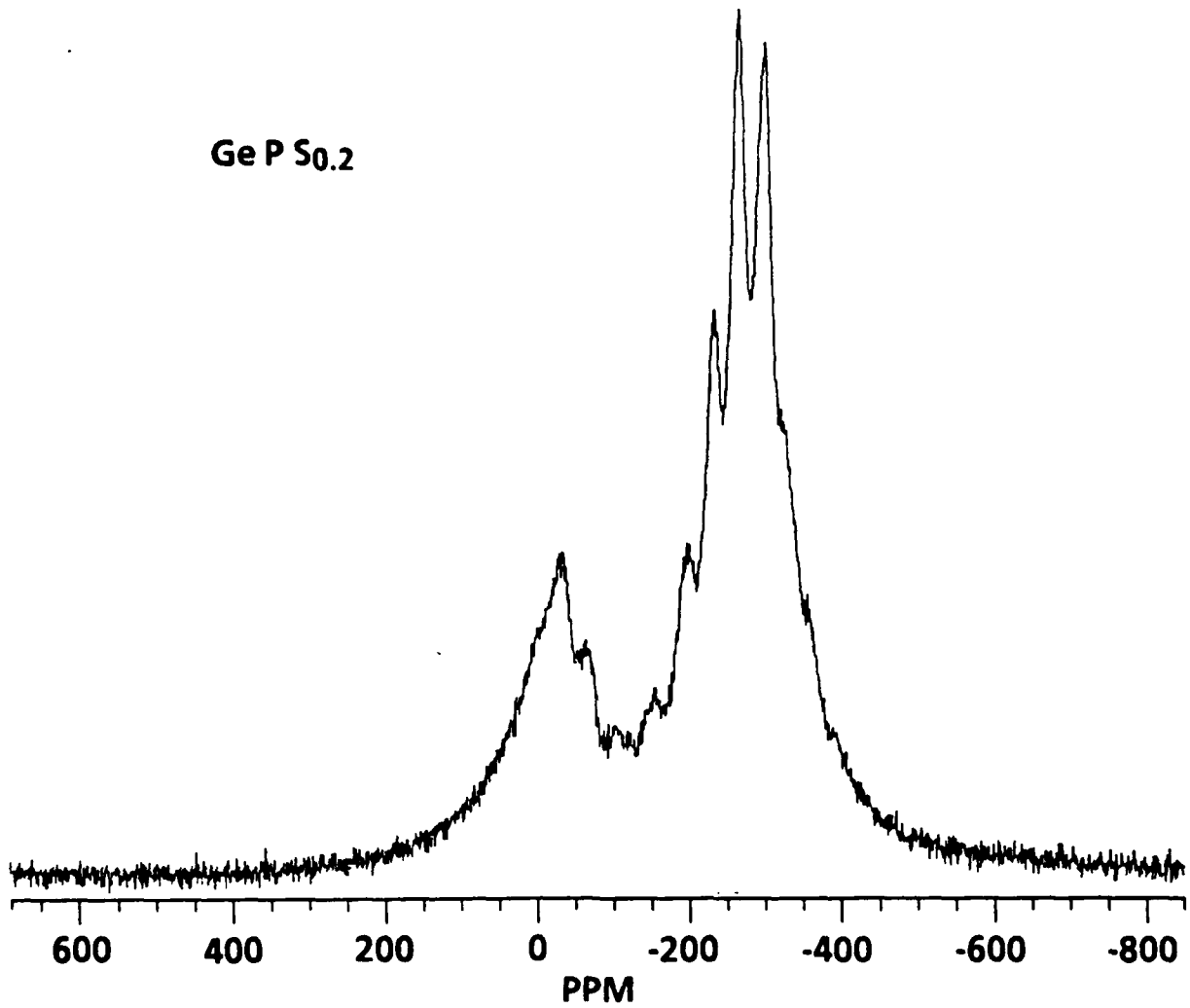


FIGURE 32. NMR SPECTRUM OF GePS<sub>0.2</sub>

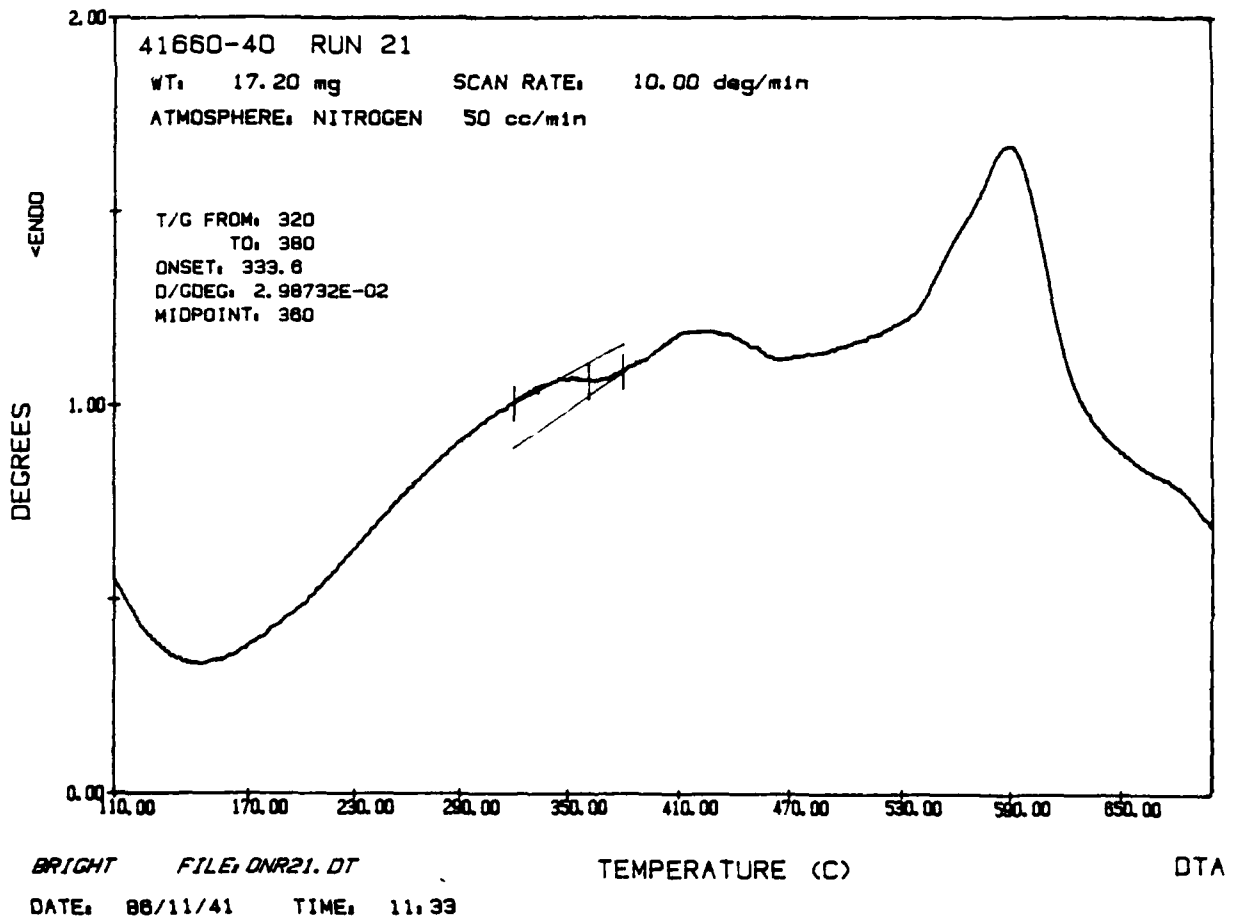
Table 5. GeZnGaPS and GeZrS Compositions Prepared

Run #	Thermal Expansion, ppm / °C	Comment	Composition,				
			Ge	Zn	Ga	S	P
17	-	Crystal	1	0.1	0.2	1.8	0.2
18	15	Crystal	1	0.2	0.2	1.6	0.4
19	12	Crystal/Glass	1	0.10	0.2	2.1	-
20	15	Crystal	1	0.05	0.2	2.05	-
21	18	Crystal	1	0.075	0.2	2.0	0.05
22	14	Crystal	1	0.1	0.2	2.3	-
23	13	Crystal	1	0.1	0.2	2.2	0.07
24	12	Crystal	1	0.1	0.2	2.3	-
25	-	Crystal	1	0.1	0.2	1.6	-
26	-	Crystal	1	0.3	0.2	1.7	0.2
27	-	Crystal	1	0.1	0.2	1.5	0.07
28	13	Crystal	1	0.1	0.2	2.3	-
	-	Crystal	1	0.016Zr	-	2.0	-
	11	Crystal	1	0.032Zr	-	2.0	-
	13	Crystal	1	0.064Zr	-	2.0	-

powder to lump changed the nature of the  $\text{GeZn}_{0.1}\text{Ga}_{0.2}\text{S}_{2.3}$  thermogram (Figure 33) with a glass transition at  $300^\circ\text{C}$ , an exotherm at  $470^\circ\text{C}$ , and a melting at  $530^\circ\text{C}$ . This indicates that the levels of oxygen found in these materials are having a significant effect on structure and properties. The phosphorus-containing materials  $\text{GeZn}_{0.075}\text{Ga}_{0.2}\text{P}_{0.05}\text{S}_2$  and  $\text{GeZn}_{0.1}\text{Ga}_{0.2}\text{P}_{0.07}\text{S}_{2.2}$  both exhibited glass transition behavior (Figures 34 and 35) in materials that were predominantly crystalline. All of the thermal expansions observed were above  $10 \text{ ppm}/^\circ\text{C}$  so attention was transferred to the alternative zirconium sulfide systems.

An attempt was made to prepare sealed tube melts in the  $\text{ZrS}_3\text{-GeS}_2$  system with ratios of 10 & 20 mole percent  $\text{ZrS}_3$ , however, in both cases variation of the temperature did not give the desired product because either the temperature was not high enough for the germanium to react or the tube exploded. At Zr:Ge ratios of up to 0.064 however glass ceramics could be prepared and their thermal expansions are given in Table 5.



FIGURE 34. DTA OF  $\text{GeZn}_{0.075}\text{Ga}_{0.2}\text{P}_{0.05}\text{S}_2$

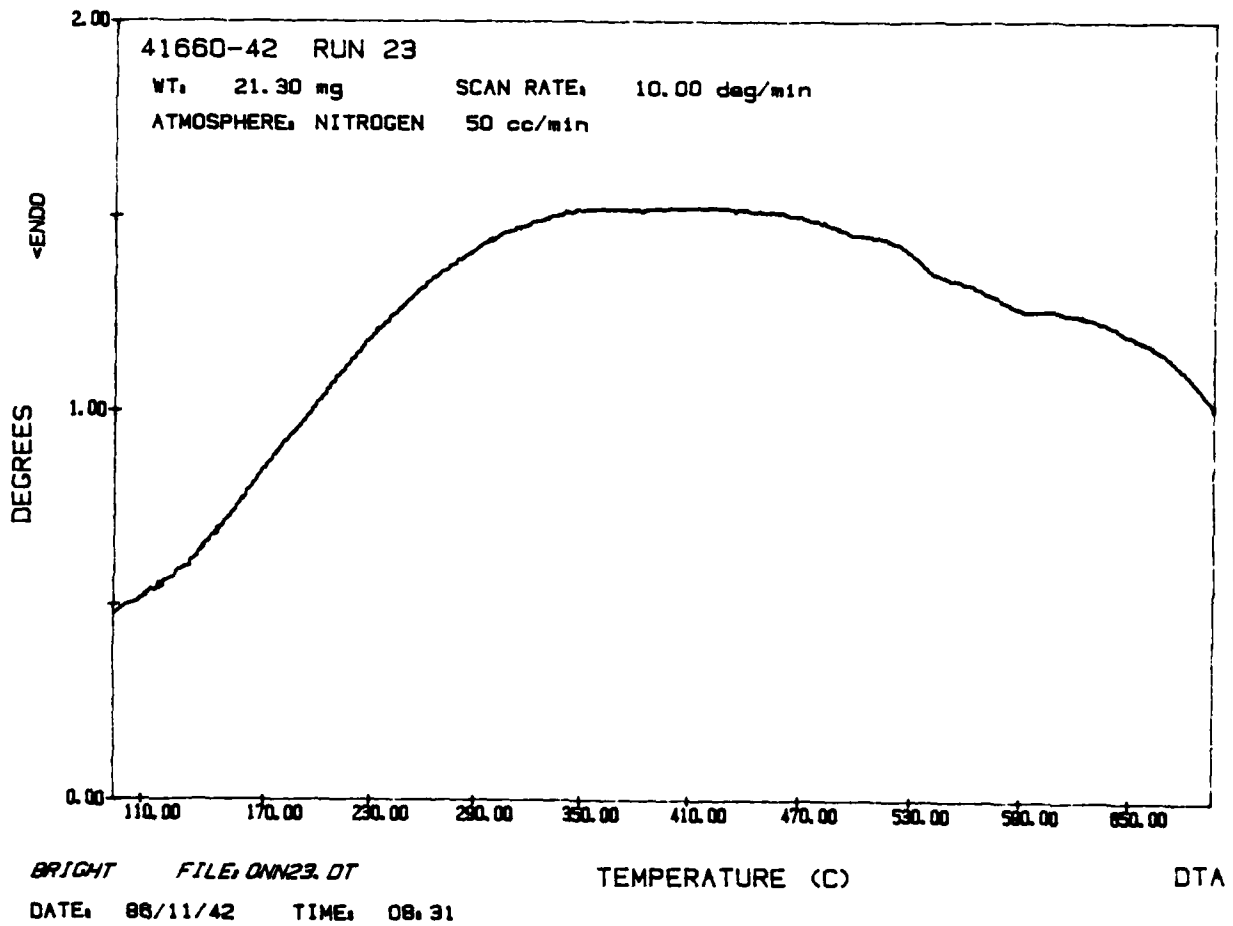


FIGURE 35. DTA OF  $\text{GeZn}_{0.1}\text{Ga}_{0.2}\text{P}_{0.07}\text{S}_{2.2}$  GLASS CERAMIC

NaLaS<sub>2</sub> Thermal Expansion

A sample of NaLaS<sub>2</sub> powder was supplied to us by Rockwell for determination of the thermal expansion coefficient. It was important to have this information because NaLaS<sub>2</sub> was being actively considered as a potential IR material and the thermal expansion coefficient is an important term in the thermal shock equation. The sample was heated at 2°C/min and XRD scans were taken over the 331, 420, 422 peaks at 20°C and at 100°C intervals between 100 and 800°C. Full scans were also taken at 200°, 400°, 600°, and 800°C. Excellent data was obtained between room temperature and 500°C (Table 6) but the sample had completely decomposed by 600°C.

TABLE 6. CALCULATION OF NaLaS<sub>2</sub> LATTICE PARAMETERS

T ( C)	2 (obs)	2 (corr)	d (angs)	a <sub>0</sub> (angs)
20	70.01	69.68	1.348	5.877
	72.07	71.74	1.315	5.879
	80.16	79.83	1.200	5.881
100	69.92	69.59	1.350	5.884
	71.96	71.63	1.316	5.887
	80.07	79.74	1.202	5.887
200	69.80	69.47	1.352	5.893
	71.87	71.54	1.318	5.893
	79.94	79.61	1.203	5.895
300	69.68	69.35	1.354	5.902
	71.74	71.41	1.320	5.903
	79.78	79.45	1.205	5.904
400	69.55	69.22	1.356	5.911
	71.62	71.29	1.322	5.911
	79.64	79.31	1.207	5.913
500	69.40	69.07	1.359	5.923
	71.48	71.15	1.324	5.921
	79.49	79.16	1.209	5.923

Figure 36 is a plot of the lattice parameter, averaged over the three determinations for each point. Regression analysis of the data gives a thermal expansion coefficient of  $15 \times 10^{-6} \text{ }^\circ\text{C}^{-1}$

### The ZnS-ZrS<sub>3</sub> System

In consultation with the program monitor it was decided that we should do some preliminary experiments to evaluate the effect of adding an IR transparent soft material (ZrS<sub>3</sub>) to the harder ZnS; it was expected that the composite would have improved toughness over the pure material. Samples were prepared by dry-milling the powders together in a Turbular mixer, and hot pressing them at 950°C to form blanks which were then machined to form test specimens. Bend strengths of pure ZnS and ZnS/ZrS<sub>3</sub> composites were determined using a 3-point test. In addition to the 3-point bend tests, a 4-point bend experiment was performed on a pure ZrS<sub>3</sub> specimen, to determine the modulus and strength of the material. The fracture toughness of the composites and of the pure ZnS material were determined using straight-notched 3-point bend specimens. In the case of the pure ZnS specimen, the load-elongation curve was linear and at the load-drop the sample broke into two pieces. In contrast, one of the composite specimens had a load-elongation curve that seemed to indicate that the crack was propagating intermittently, and also the specimen remained intact after the large load drop. Load drops were observed for the other composite specimens, but these too did not break into two when the large load drops were observed.

### Young's Modulus and Bend Strengths

Figure 37 is a stress-strain plot for the pure ZrS<sub>3</sub> specimen. Based on the initial linear portion of the stress-strain curve, a Young's modulus of 18.3 GPa (2.7 Msi) was obtained for ZrS<sub>3</sub>. The stress-strain diagram in Figure 37 also shows that the material had some non-linear deformation prior to final fracture.

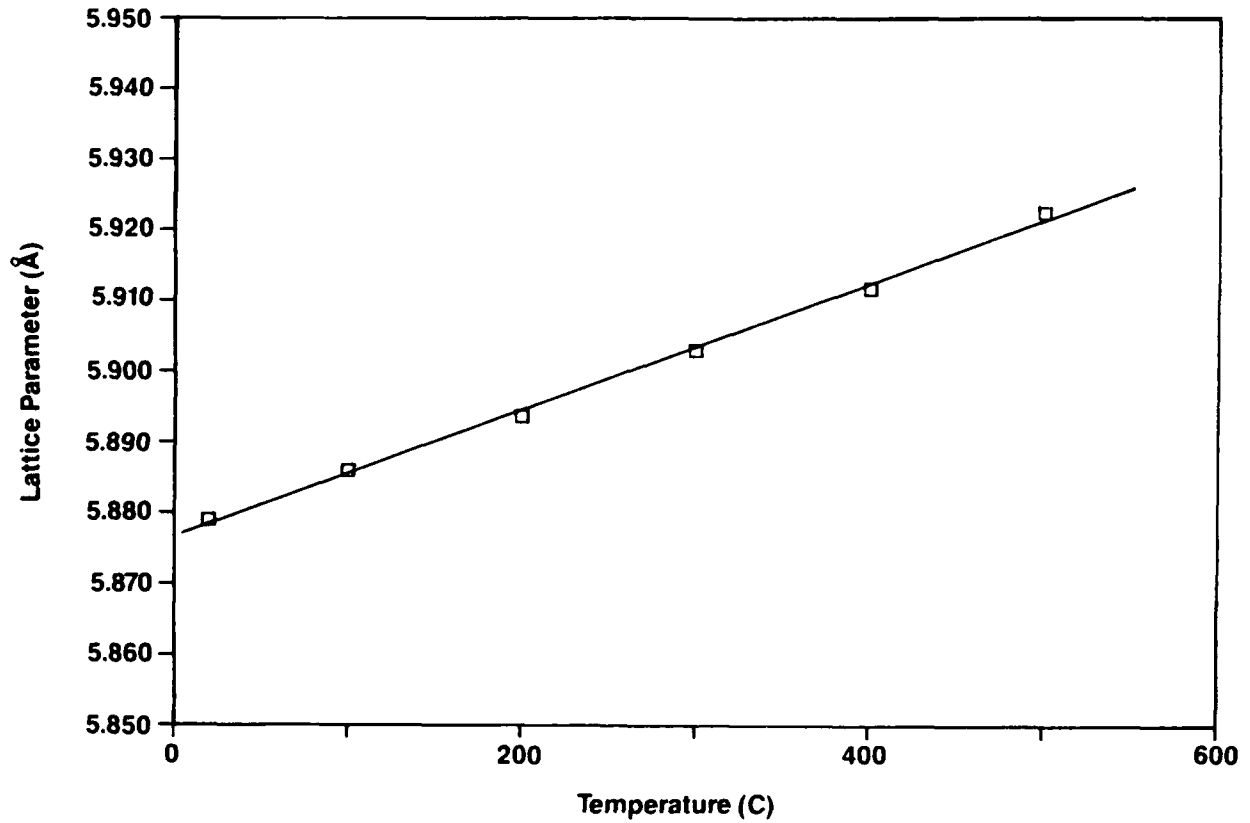
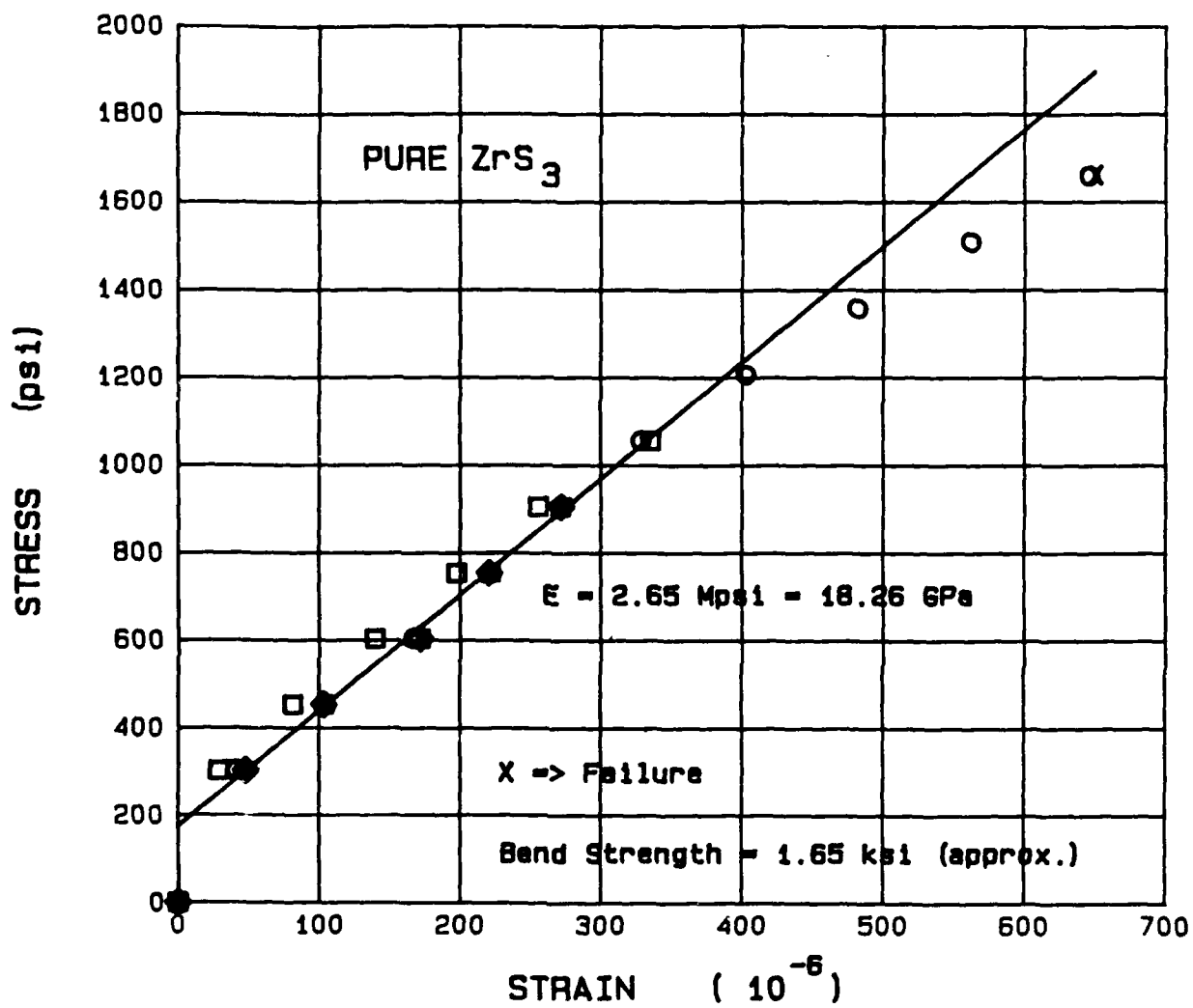
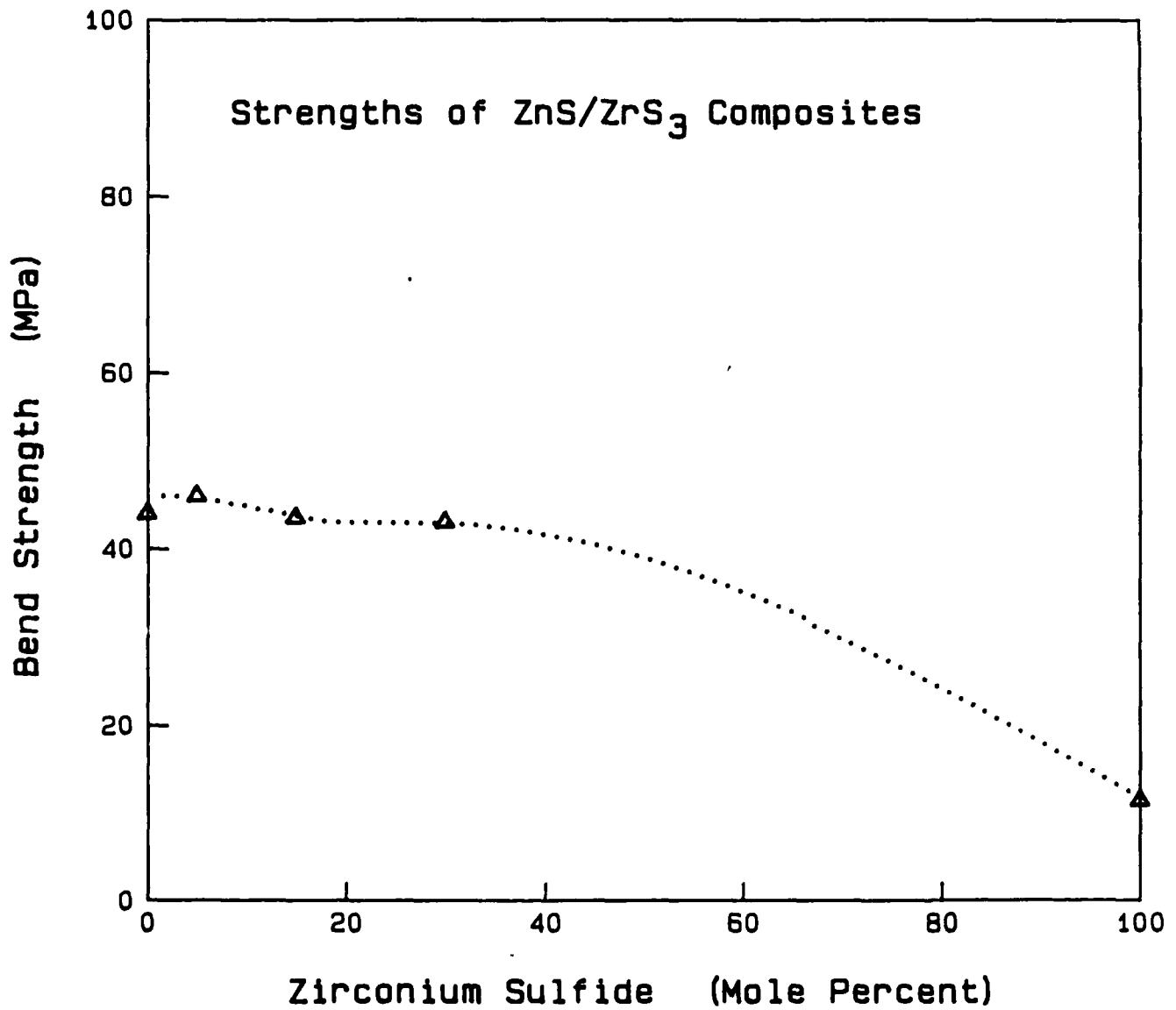


FIGURE 36. PLOT OF THE LATTICE PARAMETER OF NaLaS<sub>2</sub> POWDER AS A FUNCTION OF TEMPERATURE

FIGURE 37. STRESS-STRAIN CURVE FOR  $ZrS_3$

FIGURE 38. BEND STRENGTHS OF ZnS/ZrS<sub>3</sub> COMPOSITES

The bend strengths of the various specimens are listed in Table 7, and the data are also presented graphically in Figure 38. The data indicate that composites containing  $ZrS_3$  particulates had approximately the

TABLE 7. BEND STRENGTHS OF  $ZnS/ZrS_3$  COMPOSITES

Billet Number	$ZrS_3$ Content, Mole Percent	Bend Strength, <sup>(a)</sup>	
		MPa	ksi
43035-45	0	44	6.4 <sup>(b)</sup>
43035-43	5	46	6.7
43035-42	15	43.5	6.3
43035-41	30	43	6.2
43035-40	100	11.7	1.65 <sup>(b)</sup>

- (a) Results of duplicate specimens, unless noted.  
 (b) Only one specimen was tested.

same strength as pure ZnS, at least up to a concentration of 30-mole percent  $ZrS_3$  in ZnS. This result is interesting because pure  $ZrS_3$  had one fourth the bend strength of ZnS, and, although no quantitative measurements were made,  $ZrS_3$  was much softer than ZnS. Comparison of the load-elongation diagrams suggest that the composite specimens had Young's moduli that were lower than that of ZnS. However, since the displacements were based on measurements of only cross-head displacements, quantitative comparisons of elastic modulus could not be made.

It is also of interest to note that while the ZnS specimen failed with a flat and macroscopically smooth fracture surface, which was perpendicular to the maximum principal stress direction, the composite specimens had rougher fracture-surface morphologies. The composite specimen with 30 mole-percent  $ZrS_3$  did not break into two when the specimen was unloaded following a large load drop, and the tensile surface of the bend bar

showed a crack that was oriented at 45° to the maximum stress direction. This type of crack orientation is characteristic of shear failure, rather than the tensile brittle failure that was observed for the ZnS specimen.

### Fracture Toughness

The fracture toughness ( $K_{IC}$ ) of the materials were obtained through the formula:

$$K_{IC} = (3PL/W/2BW^2) \{ 1.93 - 3.07(a/W) + 14.53(a/W)^2 - 25.11(a/W)^3 + 25.8(a/W)^4 \} \dots (1)$$

where P is the load corresponding to fast unstable fracture, L is the span between supports for the 3-point bend fixture, W is the specimen depth, a is the crack length, and B is the thickness of the edge-notched bend specimen.

The fracture toughness of the various specimens is tabulated in Table 8. These data are plotted versus the mole percentage of  $ZrS_3$  in Figure 39.

TABLE 8. FRACTURE TOUGHNESS OF ZnS/ $ZrS_3$  COMPOSITES

Specimen Number	$ZrS_3$ Content (Mole Percent)	Fracture Toughness MPa√m
43035-45-1	0	0.59
43035-43-1	5	0.92
43035-42-1	15	0.98
43035-41-1	30	1.26

The data show that the fracture toughness of ZnS increased significantly with the addition of  $ZrS_3$  particles to the ZnS matrix. Since the load carrying capability of ceramic components and structures are ultimately governed by the fracture toughness of the material, the present results imply that, for a given applied load, the composites with  $ZrS_3$  can withstand much larger flaws

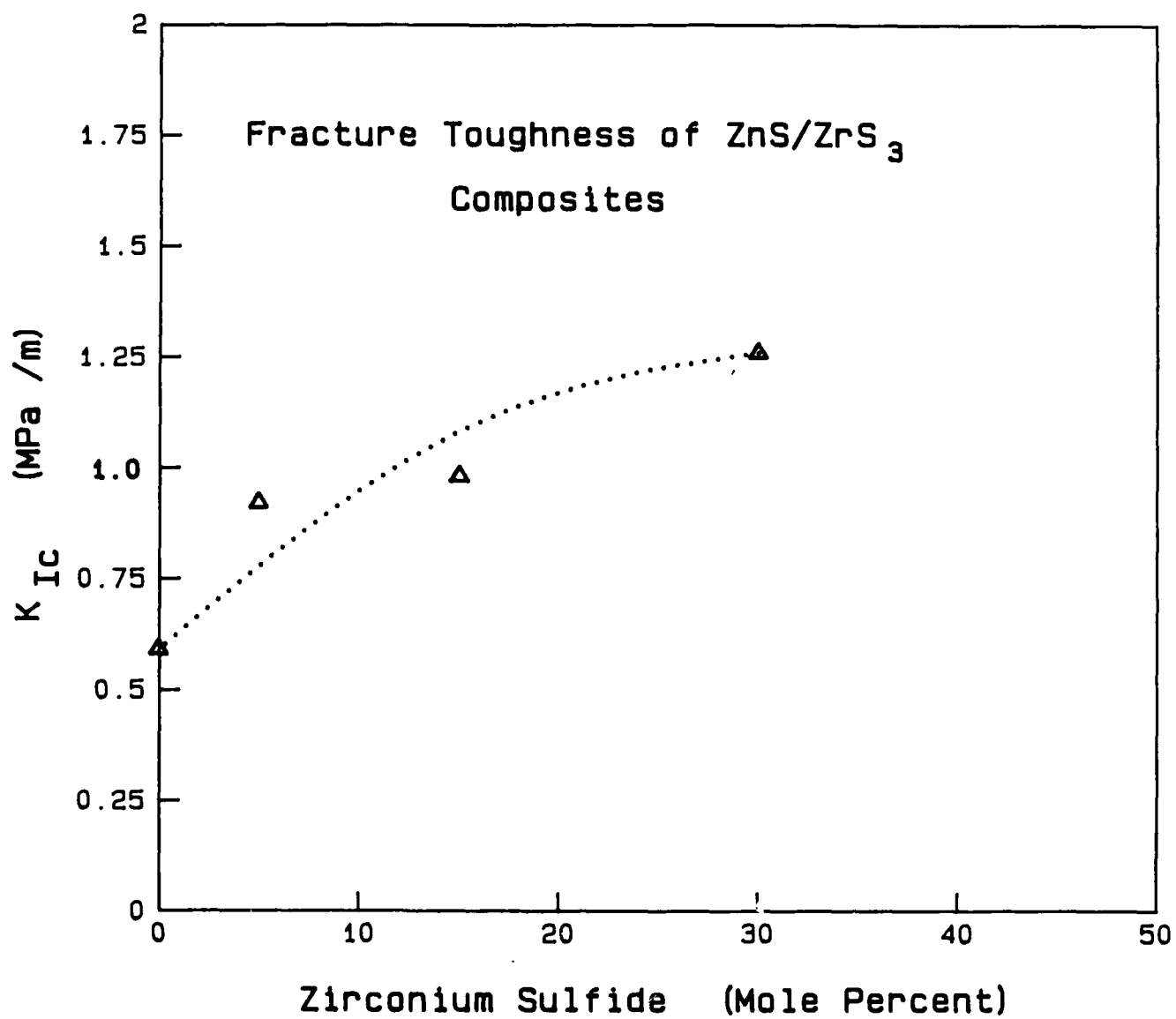


FIGURE 39. FRACTURE TOUGHNESS VERSUS MOLE % ZrS<sub>3</sub> OF ZnS/ZrS<sub>3</sub> COMPOSITES

(processing or service related) than pure ZnS. Stated in a different way, the composites are much more damage tolerant than pure ZnS.

The fracture toughness results are all the more significant because the strength data (Figure 38) showed that the addition of  $ZrS_3$  particles to ZnS did not reduce the tensile strengths. Thus, the incorporation of  $ZrS_3$  particles into a ZnS matrix can lead to significant improvements in mechanical properties. Because of the higher fracture toughness of the composites, it may be possible to obtain greater bend strengths by reducing the as-processed flaw size; for example, through the use of smaller particle sizes, or by using alternative techniques to produce a more homogeneous distribution of particles. Optimization of the processing conditions should be considered in a future research project.

### Microstructure

In order to understand the toughening mechanism for these composites, some of the cracked specimens were metallographically polished. Figure 40 shows the crack path for the 30 mole-percent fracture toughness specimen; the machined notch is visible on the left side of the micrograph. The white regions correspond to the  $ZrS_3$  particles, while the grey background corresponds to the ZnS matrix. The load elongation curve for this specimen was different from the rest of the specimens in that it had a number of small load drops, suggesting that the crack was probably propagating at loads below the final fracture load. Thus, the fast fracture  $K_{IC}$  of 1.26 MPa $\sqrt{m}$  for this specimen is probably an underestimate, because the crack length at which fast fracture occurred may have been larger than the initial machined notch length. More importantly, this type of behavior, where both the load and crack length increase with the load-point displacement, is indicative of R-curve<sup>1</sup> behavior.

---

<sup>1</sup> R-curve behavior for a material corresponds to the phenomenon of increasing fracture resistance with crack growth. The behavior is usually represented by a plot of the stress intensity factor,  $K$ , versus increase in the crack length. In a brittle material such as glass, fracture occurs in an unstable fashion at a specific value of  $K$ , and there is no R-curve behavior.



5N196

200 X

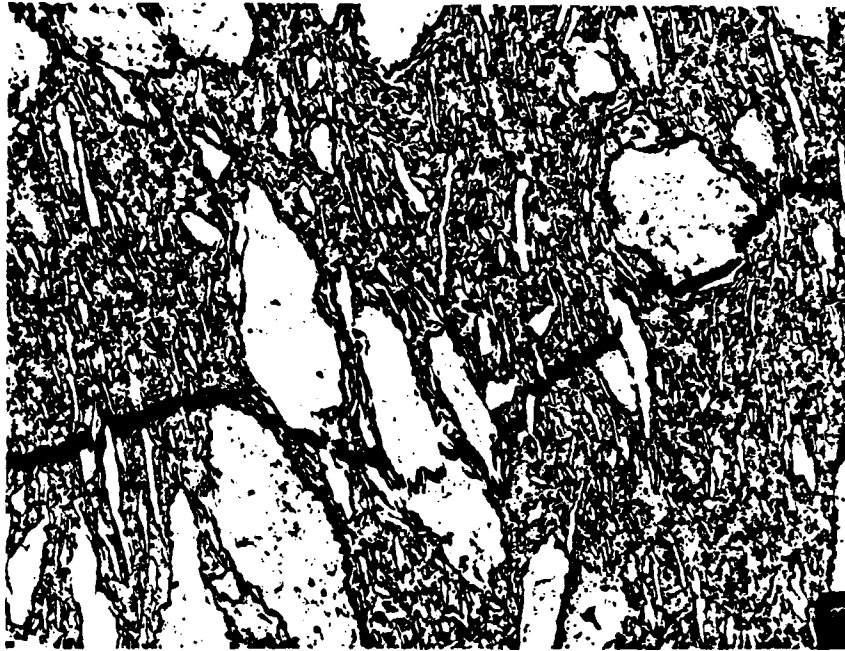
FIGURE 40. "CRACK PATH" OF 30 MOLE PERCENT  $ZrS_3$   
FRACTURE TOUGHNESS SPECIMEN

Figure 41 is a photomicrograph of the same specimen as in Figure 40 except that it is taken slightly away from the notch tip. This micrograph shows that the crack meanders around the elongated  $ZrS_3$  particles, which are actually pancake-shaped with the larger dimensions perpendicular to the plane of the micrograph. It is also very significant to note that the crack appears to be bridged by  $ZrS_3$  particles that have not fully cracked. Figure 42 is a higher magnification micrograph of a small region of Figure 41, and it shows more clearly the crack bridging phenomenon. This micrograph has been taken with polarized light, which illustrates the internal structure of the  $ZrS_3$  particles. The figure shows that the fine structure in  $ZrS_3$  can be very effective in hindering crack propagation.

#### Toughening Mechanism

Figures 40 through 42 offer a clue as to why the composite specimens had larger fracture toughness than the pure ZnS specimen. The likely scenario is that as the crack propagates it leaves behind a number of crack bridges. These bridges are either  $ZrS_3$  particles that have not cracked and that pull the crack surfaces together, or the sides of those particles which lie in the path of the crack and provide frictional resistance to the opening of the crack. The sum total effect of these stresses is to lower the effective stress intensity factor ( $K$ ) at the crack tip. Consequently, in order to obtain the matrix  $K_{Ic}$  at the crack tip, higher applied stress intensity factors become necessary. Majumdar et al<sup>(4)</sup> have recently analyzed crack bridging behavior, and one may refer to their paper for a detailed mathematical description of the crack bridging process.

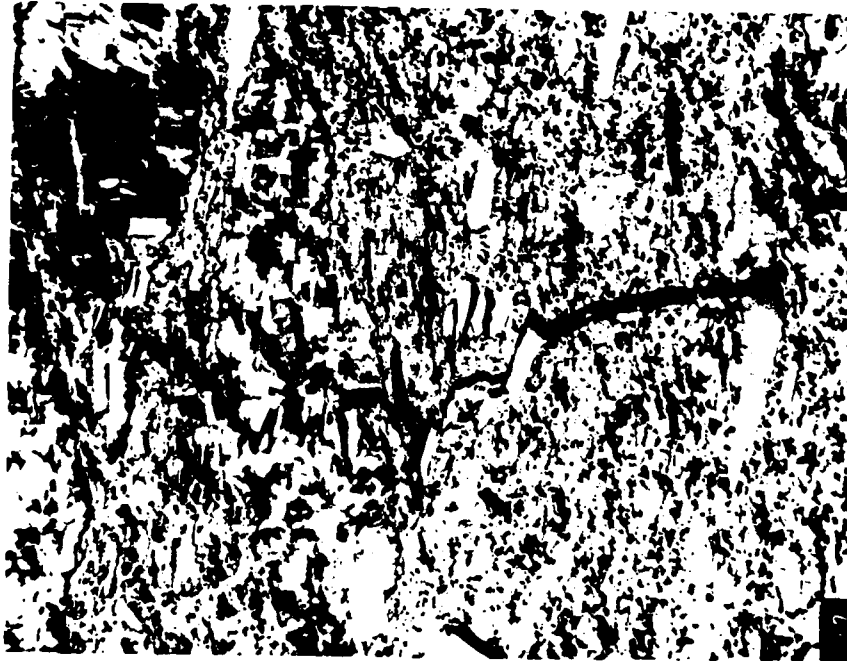
The explanation offered here is qualitatively consistent with the observed composite behavior. The number of particles bridging the crack surfaces is expected to go up with an increase in the mole percentage of particulates. Therefore, according to the present explanation, the fracture toughness should increase with an increase in the  $ZrS_3$  content. This prediction is consistent with the observed behavior (see Figure 39).



5N195

100 X

FIGURE 41. PHOTOMICROGRAPH TAKEN AWAY FROM NOTCH TIP



5N198

200 X

FIGURE 42. HIGHER MAGNIFICATION OF SMALL REGION  
OF FIGURE 41

## CONCLUSIONS

In this work a large number of new glass and glass-ceramic compositions have been surveyed but we have not been able to identify any serious new competitors to ZnS as a LWIR infra-red dome material. An important result has been obtained with the demonstration of substantial toughening, without loss in strength, of hot-pressed ZnS by the addition of the softer, weaker, material  $ZrS_3$ . This result suggests a line of approach that should prove to be profitable if pursued.

The results from the work on the GeGaPS and GeZnGaPS phase diagrams have revealed a large number of new and scientifically interesting glasses and glass ceramics. A highly complex crystallization behavior was observed in the  $GeGa_{0.24}P_{0.2}S_{2.0}$  glass with mixed crystals, indicating solid solution behavior, and highly varied crystal morphologies observed. While the measured thermal expansions were too high for the requirements of this program the zinc containing glass ceramic system merits further study. Additions of the alkaline earths to the basic composition to increase melting temperatures also merit study but the resources on this program did not permit investigation. From this initial survey it appears that the sialon structure does not readily form with these components.

The wisdom of a glass ceramic or multiphase composite approach has been demonstrated by the mechanical testing results obtained with hot-pressed  $ZrS_3$ -ZnS composites. With no attempt at optimization and with a large particle sized  $ZrS_3$  powder we obtained increases in fracture toughness of over a factor of two without loss in strength. This implies an increase in the size of the critical flaw so it is highly likely that reduction in the particle size of the  $ZrS_3$  powder will lead to increased strength as well.

## REFERENCES

1. Frerichs, R., Phys. Rev., 78, 643 (1950).
2. Frerichs, R., J. Opt. Soc. Am., 43, 1153 (1953).
3. Hilton, A. R., "New High Temperature Infrared Transmitting Glasses", DTIC Rep. AD623262 (1965).
4. Majumdar, B. S., Rosenfield, A. R., and Duckworth, W. H., "Analysis of R-Curve Behavior of Non-Phase-Transforming Ceramics", Engineering Fracture Mechanics, 31, 683-701 (1988).